

# $^{40}\text{Ar}/^{39}\text{Ar}$ ages and palaeomagnetism of transitionally magnetized volcanic rocks in the Society Islands, French Polynesia: Raiatea excursion in the upper-Gauss Chron

Y. Yamamoto,<sup>1</sup> O. Ishizuka,<sup>2</sup> M. Sudo<sup>3</sup> and K. Uto<sup>2</sup>

<sup>1</sup>Geomagnetism Laboratory, Department of Earth and Ocean Sciences, University of Liverpool, Oliver Lodge Laboratories, Oxford Street, Liverpool L69 7ZE, United Kingdom. E-mail: y.yamamoto@liverpool.ac.uk

<sup>2</sup>Geological Survey of Japan, AIST, Tsukuba 305-8567, Japan

<sup>3</sup>Institute of Earth Sciences, University of Potsdam, Karl-Liebknechtstrasse 24, Haus 27, 14476 Golm, Germany

Accepted 2006 October 18. Received 2006 October 18; in original form 2006 September 17

## SUMMARY

Volcanic rock samples from several sites in the Society Islands, French Polynesia were found to be transitionally magnetized. To better characterize these geomagnetic events, we performed laser-heating  $^{40}\text{Ar}/^{39}\text{Ar}$  dating and additional palaeomagnetic measurements on these samples. The measurements give virtual geomagnetic pole (VGP) latitudes of 0.7–52.4°N and virtual dipole moment (VDM) values of  $0.433\text{--}0.682 \times 10^{22}$  A m<sup>2</sup> which are typical for the transitional geomagnetic field. These transitional events occurred at  $2.77 \pm 0.02$  Ma (Raiatea),  $3.20 \pm 0.03$  Ma (Tahaa) and  $4.40 \pm 0.01$  Ma (Maupiti). Considering the reported radioisotopic ages for known geomagnetic events, it is suggested the first event is a previously unknown geomagnetic excursion (Raiatea excursion) while the latter two probably correspond to known polarity transitions (upper boundary ages of the Mammoth reversed subchron and the Nuni-vak normal subchron). The existence of the proposed Raiatea excursion is supported by the contemporaneous palaeointensity low recognized in the relative palaeointensity stack from the equatorial Pacific.

**Key words:**  $^{40}\text{Ar}/^{39}\text{Ar}$  dating, geomagnetic excursion, palaeointensity.

## 1 INTRODUCTION

The geomagnetic field varies with time and the accumulation of palaeomagnetic data has revealed that the field has experienced numerous polarity reversals. The geomagnetic polarity timescale (GPTS) compiled by Cande & Kent (1995) suggests that 20 reversals occurred during the last 5 Myr, which is equivalent to a frequency of one reversal per 250 kyr. However, the last reversal occurred at  $776 \pm 2$  kyr (Singer *et al.* 2005) with a normal polarity period (Brunhes Chron) continuing to the present day. The Brunhes Chron is considered to be an extraordinarily long-polarity period when compared with the other geomagnetic chrons of the last 5 Myr. Tauxe (2006) pointed out that the average geomagnetic dipole moment appears to be substantially less than the present day value ( $\sim 8 \times 10^{22}$  A m<sup>2</sup>) except for the Brunhes and the longest polarity intervals like the Cretaceous Normal Superchron. This conclusion is consistent with a longstanding hypothesis that strong field may tend to prevent the geomagnetic field from reversing its polarity (e.g. Cox 1968).

It might be thought that as the geomagnetic field is very stable during the Brunhes Chron that the geomagnetic pole has kept its position close to the geographic pole since the last reversal. This is not the case as there have been many studies reporting occurrences of geomagnetic excursions during the Brunhes Chron. A geomagnetic

excursion is characterized by a large swing of the palaeomagnetic field vector which exceeds the limit of palaeosecular variation but then returns to its original polarity. It is thus distinct from a full polarity reversal and lasts for few thousand years. Oda (2005) extensively compiled excursion records from the literature. He concluded that probably more than 18 (possibly up to 23) excursions occurred during the Brunhes Chron, and most of them are associated with relative palaeointensity lows.

Occurrences of geomagnetic excursions are not limited to the Brunhes Chron. Singer & Brown (2002) compiled the GPTS for the upper-Matuyama Chron based on  $^{40}\text{Ar}/^{39}\text{Ar}$  ages from terrestrial lavas. They reported excursions at  $0.899 \pm 0.003$  Ma (Kamikatsura event),  $0.936 \pm 0.004$  Ma (Santa Rosa event),  $1.122 \pm 0.005$  Ma (Punaruu event) and  $1.194 \pm 0.007$  Ma (Cobb Mountain event) relative to 28.34 Ma Taylor Creek rhyolite Sanidine (TCS) or 28.02 Ma Fish Canyon Tuff Sanidine (FCTS). Coe *et al.* (2004) studied 81 basaltic lava flows from the northwest wall of Haleakala caldera, Maui, finding the Kamikatsura event with  $^{40}\text{Ar}/^{39}\text{Ar}$  age of  $0.9004 \pm 0.0046$  Ma (relative to 28.34 Ma TCS). This age is a revised one that includes their previous results from Tahiti (Singer *et al.* 1999; Singer & Brown 2002).  $^{40}\text{Ar}/^{39}\text{Ar}$  ages for the Cobb Mountain event were also reported as  $1.18 \pm 0.02$  Ma (27.92 Ma TCS) by Tanaka *et al.* (1996) and  $1.186 \pm 0.006$  Ma (27.84 Ma FCTS) by Turrin

**Table 1.** Compiled timing of the reported geomagnetic excursions in Matuyama chron (radiometric ages).

Excursion	Age (Ma, $\pm 1\sigma$ )	(original)	Method	Reference
Kamikatsura	<b>0.8837 <math>\pm</math> 0.0045</b>	(0.9004)	$^{40}\text{Ar}/^{39}\text{Ar}$ , global mean	Coe <i>et al.</i> (2004)
Santa Rosa	<b>0.919 <math>\pm</math> 0.004</b>	(0.936)	$^{40}\text{Ar}/^{39}\text{Ar}$ , direct	Singer & Brown (2002)
Punaruu	<b>1.101 <math>\pm</math> 0.005</b>	(1.122)	$^{40}\text{Ar}/^{39}\text{Ar}$ , direct	Singer & Brown (2002)
Cobb Mountain	1.172 $\pm$ 0.006	(1.186)	$^{40}\text{Ar}/^{39}\text{Ar}$ , direct	Turrin <i>et al.</i> (1994)
	1.18 $\pm$ 0.02		$^{40}\text{Ar}/^{39}\text{Ar}$ , direct	Tanaka <i>et al.</i> (1996)
	1.172 $\pm$ 0.007	(1.194)	$^{40}\text{Ar}/^{39}\text{Ar}$ , direct	Singer & Brown (2002)
	<b>1.17</b>			
Gilsa	<b>1.62 <math>\pm</math> 0.04</b>		K-Ar, ditrect	Udagawa <i>et al.</i> (1999)
Reunion II (Huckleberry Ridge)	<b>2.059 <math>\pm</math> 0.004</b>		$^{40}\text{Ar}/^{39}\text{Ar}$ , direct	Lanphere <i>et al.</i> (2002)
Reunion top	2.11 $\pm$ 0.04		K-Ar, interpolation	McDougall <i>et al.</i> (1992)
	2.12 $\pm$ 0.04		$^{40}\text{Ar}/^{39}\text{Ar}$ , direct	Baksi <i>et al.</i> (1993)
	2.05 $\pm$ 0.01	(2.09)	$^{40}\text{Ar}/^{39}\text{Ar}$ , extrapolation	Roger <i>et al.</i> (2000)
	<b>2.12</b>			
Reunion bottom	2.15 $\pm$ 0.04		K-Ar, interpolation	McDougall <i>et al.</i> (1992)
	2.15 $\pm$ 0.03		$^{40}\text{Ar}/^{39}\text{Ar}$ , direct	Roger <i>et al.</i> (2000)
	<b>2.15</b>			

Ages in bold face are compiled timing of the geomagnetic excursions (arithmetic means are indicated if there are multiple reported ages for one excursion).  $^{40}\text{Ar}/^{39}\text{Ar}$  ages are recalculated relative to 27.5 Ma FCTS or 27.92 Ma TCS. Original  $^{40}\text{Ar}/^{39}\text{Ar}$  ages are indicated in parentheses if recalculations were made.

*et al.* (1994). As for the lower Matuyama Chron, Udagawa *et al.* (1999) observed two normally magnetized lavas bracketed by ones with reversed directions. They concluded that these lavas recorded the Gilsa event, with mean K-Ar age of  $1.62 \pm 0.04$  Ma. Lanphere *et al.* (2002) dated the Huckleberry Ridge Tuff with a transitional magnetic direction that had previously been related to the Reunion event. Since its mean  $^{40}\text{Ar}/^{39}\text{Ar}$  age of  $2.059 \pm 0.004$  Ma (27.92 Ma TCS) was significantly younger than the Reunion event, they suggested this as a new event.  $^{40}\text{Ar}/^{39}\text{Ar}$  ages of the Reunion event were previously reported as  $2.12 \pm 0.04$  Ma (27.92 Ma TCS; Baksi *et al.* 1993) and  $2.09 \pm 0.01$  Ma (28.02 Ma FCTS; Roger *et al.* 2000) for the top, and  $2.15 \pm 0.03$  Ma (Baksi *et al.* 1993) for the bottom. The ages of these excursions are compiled in Table 1 (note that the  $^{40}\text{Ar}/^{39}\text{Ar}$  ages are recalculated relative to 27.5 Ma FCTS or 27.92 Ma TCS, see Section 3.1).

The compilation in Table 1 is limited to radiometric ages from terrestrial materials. Additional excursion records from lake or deep sea sediments can be found in the literature. For example, Yamazaki & Oda (2005) constructed a relative palaeointensity stack between 0.8 and 3.0 Ma (EPAPIS-3 Ma) from six sediment cores taken from the equatorial Pacific. They found quasi-periodic palaeointensity lows in the stack and reported that parts of the palaeointensity minima seem to be accompanied by geomagnetic excursions. Similar quasi-periodic lows can also be found in the relative palaeointensity stack for the last 2 Myr (Sint-2000; Valet *et al.* 2005). It seems reasonable that geomagnetic excursions may be recurrent through Earth history and that the existence of frequent lows in relative palaeointensity could be correlated with unknown geomagnetic excursions. It is, therefore, important to study possible geomagnetic excursion records of all ages to build-up a catalogue of excursions in order to enhance our knowledge of the geomagnetic field.

In Yamamoto *et al.* (2002) and Yamamoto & Tsunakawa (2005), volcanic rock samples from several sites in the Society Islands, French Polynesia were found to be transitionally magnetized and which may be recording previously unknown geomagnetic excursions.

To constrain the age of these samples, laser-heating  $^{40}\text{Ar}/^{39}\text{Ar}$  dating was performed. New palaeomagnetic measurements were also conducted to enhance data quality. The results of these experiments are reported in this paper.

## 2 SAMPLES

The Society Islands consist of 10 volcanic islands and several seamounts formed by hotspot activity. The current hotspot is comprised of the submarine flank of Mehetia Island and several seamounts (e.g. Volcano 16: 18.28°S, 148.17°W; Binard *et al.* 1991). Yamamoto *et al.* (2002) reported 130 palaeomagnetic direction data from seven of the Society Islands. In their study, 10 intermediate palaeodirections were found: five directions from six consecutive lavas on Raiatea Island (RT04, 05, 06, 07, 10 and 11), four directions from four concordant lava flows on Tahaa Island (TA04, 05, 06 and 07), and one direction from a dyke on Maupiti Island (MP01). Samples from these sites collected at the same time as those used in the Yamamoto *et al.* study were used for the present measurements. Sampling sites are shown in Fig. 1.

## 3 $^{40}\text{AR}/^{39}\text{AR}$ DATING

### 3.1 Experiment and data analysis

Age determination was made using the laser-heating  $^{40}\text{Ar}/^{39}\text{Ar}$  system at the Geological Survey of Japan (GSJ), AIST (Uto *et al.* 1997). Rock samples were gently crushed into 30–60 mesh grains and ultrasonically cleaned in distilled water. The samples were then treated ultrasonically in 3M HCl for 10 min to remove any possible alteration products before being again cleaned ultrasonically in distilled water, and subsequently dried in air. After these treatments, groundmasses were extracted from the cleaned grains by an isodynamic separator and wrapped in aluminium foil packets of around  $2 \times 2$  mm in size. The packets were stacked in a pure

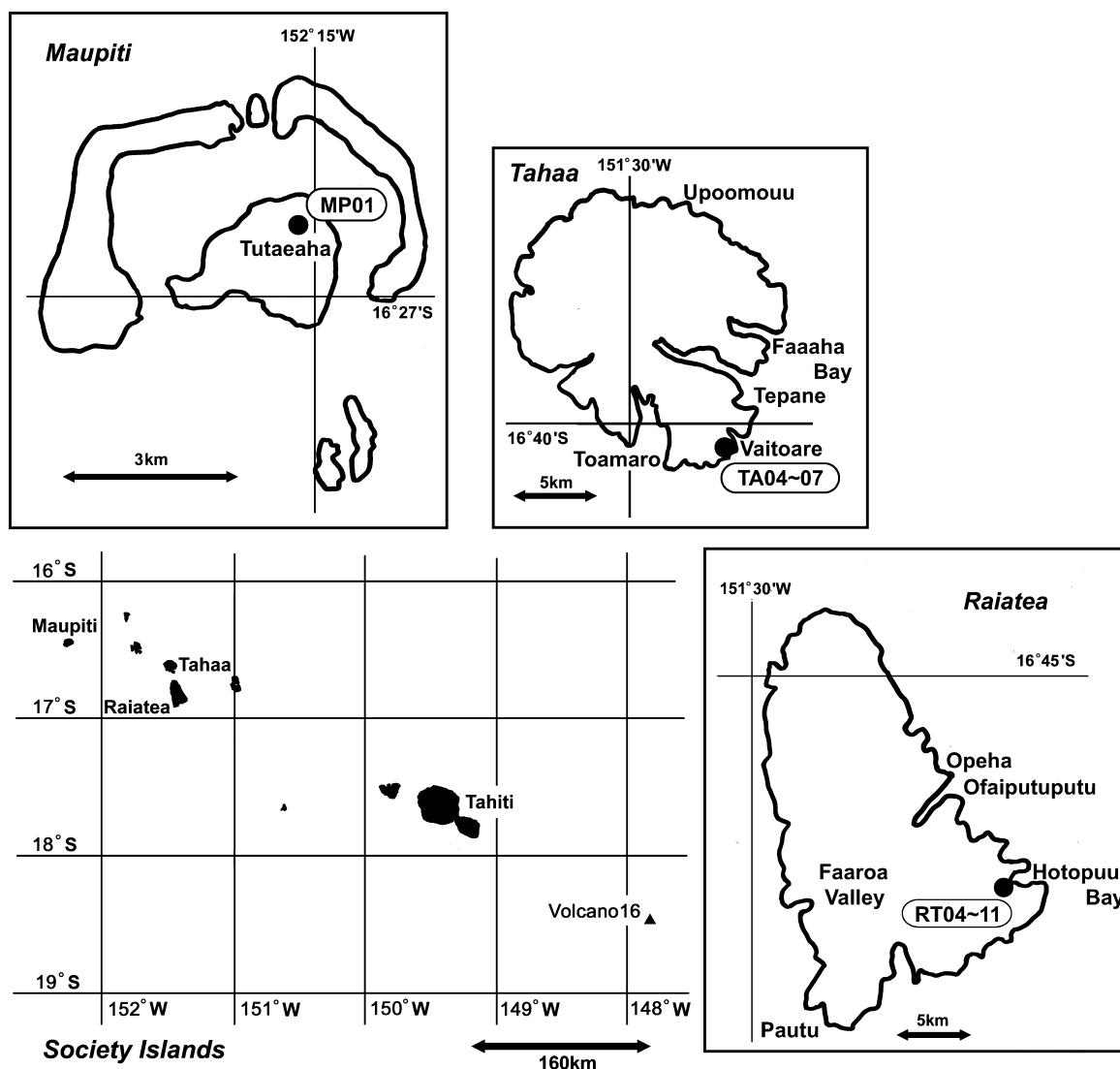


Figure 1. Map showing the sampling sites. The Volcano 16 (18.28°S, 148.17°W; Binard *et al.* 1991) is one of the seamounts comprising the Society hotspot.

aluminium irradiation capsule with flux monitor minerals of Fish Canyon Tuff sanidines (FCTS; Steven *et al.* 1967; Lipman 1975; Whiteny & Stormer 1985). In the GSJ laboratory, an age for FCTS was adopted as 27.5 Ma (Ishizuka *et al.* 2003). This is based on the calibration against the primary standard for the K-Ar laboratory at GSJ (Sori biotite, 91.2 Ma; Uchiumi & Shibata 1980). The age for FCTS is consistent with the best age suggested by Lanphere & Baadsgaard (2001) (27.51 Ma). Samples were irradiated at the JMTR reactor with fast neutron flux of about  $6.7 \times 10^{12}$  neutrons  $\text{cm}^{-2} \text{s}^{-1}$  (Ishizuka 1998). Interfering isotopes were corrected on the basis of analytical results of  $\text{CaFeSi}_2\text{O}_6$  and  $\text{KFeSiO}_4$  glasses irradiated with the samples.

In the measurement, the samples were heated stepwise by a continuous Ar ion laser. The laser was exposed for three minutes in each step, and extracted gas was purified for 10 min with Zr-Al and Zr-Fe-V getters. Ar isotopes were measured on the VG Isotech VG3600 noble gas mass spectrometer. Mass discrimination was monitored using diluted air. The blank analysis was conducted after every three or four analysis steps.

From the obtained results, plateau ages were determined following Fleck *et al.* (1977). They were calculated as weighted averages from the ages of the plateau-forming steps. Inverse isochrons

were calculated from the same step data using York's least-square fit (York 1969). If analytical results fulfilled the following criteria (e.g. Lanphere & Dalrymple 1978; Dalrymple *et al.* 1980), the plateau ages were regarded as reliable.

- (i) A plateau consists of more than three sequential steps and 50 per cent of  $^{39}\text{Ar}$  released. The ages of each step should be concordant within two standard deviations ( $\pm 2\sigma$ ).
- (ii) An inverse isochron from the plateau-forming step data should exist with the  $^{40}\text{Ar}/^{39}\text{Ar}$  intercept not different from 295.5 at the  $2\sigma$  level.
- (iii) The plateau age and the inverse isochron age should be consistent within two standard deviations ( $\pm 2\sigma$ ).

The details of the system and the experimental and analytical procedures are described in Ishizuka *et al.* (2003).

### 3.2 Results

Samples from five sites (RT05, RT10, TA04, TA05 and MP01) underwent age determination. The resultant  $^{40}\text{Ar}/^{39}\text{Ar}$  age spectra and associated Ca/K plots are displayed in Fig. 2. The analytical results

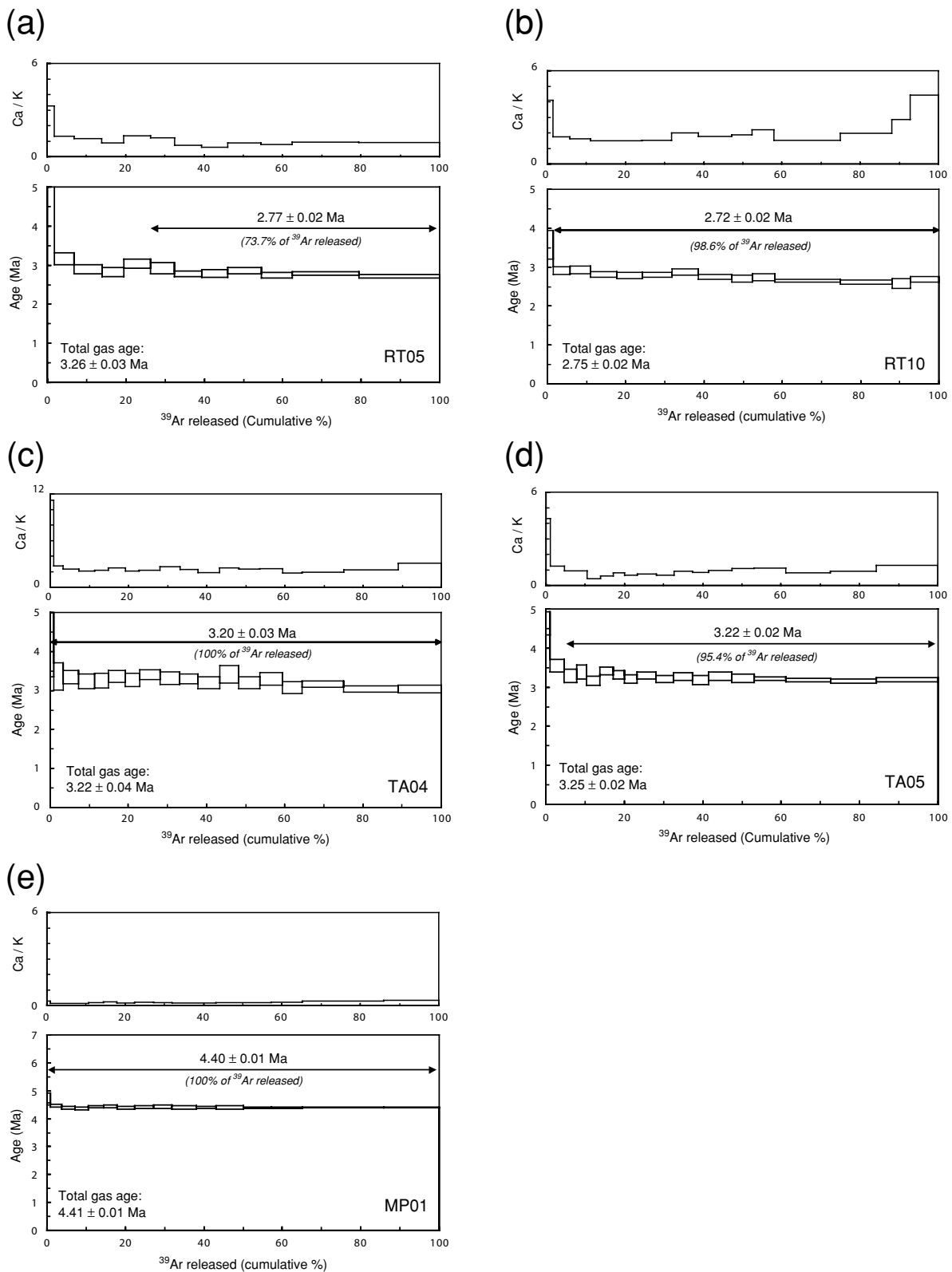


**Figure 2.**  $^{40}\text{Ar}/^{39}\text{Ar}$  age spectra with Ca/K plots. (a) RT05, (b) RT10, (c) TA04, (d) TA05 and (e) MP01.

are summarized in Table 2 (detailed results of isotopic analysis for each sample are indicated in Appendix A).

Plateau ages were obtained from almost the entire fraction of  $^{39}\text{Ar}$  released for all samples apart from RT05 (Figs 2b–e). Even for RT05,

the plateau consisted of 73.7 per cent of  $^{39}\text{Ar}$  released (Fig. 2a) hence the present dating seems to be of good quality. However, inverse isochrons of plateau-forming steps from RT10 and TA05 yielded  $^{40}\text{Ar}/^{39}\text{Ar}$  intercepts of  $433 \pm 46$  and  $351 \pm 26$  (Table 2), which

**Table 2.**  $^{40}\text{Ar}/^{39}\text{Ar}$  dating results.

Site	Total gas age (Ma)	Plateau age ( $\pm 1\sigma$ )				
		Weighted average (Ma)	Inv. Isochron age (Ma)	$^{40}\text{Ar}/^{36}\text{Ar}$ intercept	MSWD	Fraction of $^{39}\text{Ar}$ (per cent)
RT05	3.26 $\pm$ 0.03	<b>2.77 <math>\pm</math> 0.02</b>	2.73 $\pm$ 0.04	302 $\pm$ 6	0.77	73.7
RT10	2.75 $\pm$ 0.02	2.72 $\pm$ 0.02	2.56 $\pm$ 0.06	433 $\pm$ 46	1.10	98.6
TA04	3.22 $\pm$ 0.04	<b>3.20 <math>\pm</math> 0.03</b>	2.83 $\pm$ 0.16	465 $\pm$ 90	0.77	100.0
TA05	3.25 $\pm$ 0.02	3.22 $\pm$ 0.02	3.05 $\pm$ 0.08	351 $\pm$ 26	0.61	95.4
MP01	4.41 $\pm$ 0.01	<b>4.40 <math>\pm</math> 0.01</b>	4.39 $\pm$ 0.02	342 $\pm$ 25	0.53	100.0

Inv. Isochron age, inverse isochron age; MSWD, mean square of weighted deviates ( $\sqrt{\frac{\text{SUMS}}{n-2}}$ ) in York (1969). All errors are indicated by one standard deviation ( $\pm 1\sigma$ ). Integrated ages were calculated using sum of the total gas released. Weighted averaged ages in boldface fulfilled reliability criteria (see text).  $\lambda_\beta = 4.962 \times 10^{-10} \text{ yr}^{-1}$ ,  $\lambda_e = 0.581 \times 10^{-10} \text{ yr}^{-1}$ ,  $^{40}\text{K}/\text{K} = 0.01167$  per cent (Steiger & Jäger 1977).

are significantly higher than atmospheric ratio (295.5). As these intercepts imply the possible presence of excess  $^{40}\text{Ar}$ , the results from RT10 and TA05 were discarded from further discussion. The other three plateau ages of  $2.77 \pm 0.02$ ,  $3.20 \pm 0.03$  and  $4.40 \pm 0.01$  Ma from RT05, TA04 and MP01 fulfilled the reliability criteria, respectively.

The K-Ar ages reported in the literature can be summarized as 2.29–3.17 Ma for Raiatea, 2.62–3.39 Ma for Tahaa (except for two data), and 3.94–4.85 Ma for Maupiti (Fig. 3) (Duncan & McDougall 1976; Roperch & Duncan 1990; Diraison 1991; White & Duncan 1996; Blais *et al.* 1997; Guillou *et al.* 1998). These ages are concentrated around 2.5 Ma (Raiatea), 3.0 Ma (Tahaa) and 4.5 Ma

(Maupiti). The  $^{40}\text{Ar}/^{39}\text{Ar}$  ages obtained in the present study are consistent with the reported K-Ar ages (Fig. 3).

## 4 MAGNETIC MEASUREMENT

### 4.1 Rockmagnetic properties

Rock magnetic properties provide important information for palaeomagnetic measurements. We carried out hysteresis measurements at room temperature, and susceptibility measurements at high temperature.

The hysteresis parameters saturation magnetization (Ms), remanent saturation magnetization (Mrs), coercivity (Bc) and remanent coercivity (Brc) were measured for 44 small chips from 14 selected palaeomagnetic cores. Measurements were conducted on several chips for each core, three on average, using a vibrating sample magnetometer (MicroMag 3900 VSM, Princeton Measurement Corporation) or an alternating gradient force magnetometer (MicroMag 2900 AGFM, PMC). Core-averaged hysteresis parameters are listed in Tables 3–5, and the resultant Day plot (Day *et al.* 1977; Dunlop 2002) is shown in Fig. 4. It is seen that the data points are generally distributed along SD (single domain) and MD (multidomain) mixing curves of magnetite (after Dunlop 2002). This implies that the remanence carriers of the present samples are admixtures of SD (and/or PSD) and MD, and their compositions are close to magnetite (Ti-free titanomagnetite, TM0). Compositions of Ti-poor titanomagnetites (e.g.  $\sim$ TM10) are also probable scenarios because some data points are slightly offset from the mixing curves (Fig. 4).

We performed FORC (first-order reversal curve; Roberts *et al.* 2000) measurements using the AGFM on specimens from five selected cores. The FORC diagrams obtained are displayed in Fig. 4. Apart from the result of MP01-03, SD-like contributions are clearly recognized by the number of closing contours (Figs 4a, c, d and e). Centres of the contours (peaks) are locating at  $H_c \sim 15$  to 40 mT. Even for MP01-03, there are elongated contours reaching  $H_c \sim 140$  mT along the axis of  $H_u = 0$  (Fig. 4f), indicative of an SD contribution. These SD components probably originate from deuteric oxidation of titanomagnetite (TM) grains. This is supported by the fact that a number of TM grains associated with exsolved ilmenite lamellae were observed in a thin section of sample RT10-04 (Fig. 4b), and the hysteresis data plotted on the Day plot lies approximately along the SD–MD mixing curves together with the data from the other samples (Fig. 4). Variation in hysteresis parameters as shown on the Day plot probably relates to the degree of deuteric oxidation with

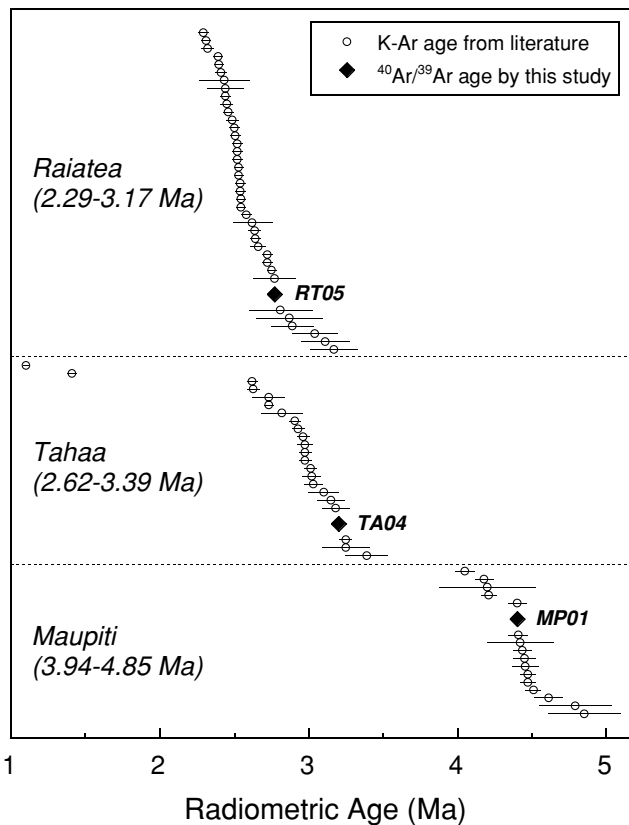


**Figure 3.** K-Ar ages reported from Raiatea, Tahaa and Maupiti samples in the literature (open circles), and  $^{40}\text{Ar}/^{39}\text{Ar}$  ages obtained in this study (closed diamonds). Error bars are indicated at the  $1\sigma$  level.

**Table 3.** Results of the LTD-DHT Shaw palaeointensities for the Raiatea samples.

Sample ID	NRM <sub>0</sub>	ARM0 <sub>0</sub>	B <sub>rc</sub> /B <sub>c</sub>	M <sub>rs</sub> /M <sub>s</sub>	LTD (per cent)	First heating				Second heating				F <sub>L</sub> (μT)	F (μT)	ΔAIC		
						H <sub>L</sub>	slope <sub>A1</sub>	slope <sub>N</sub>	f <sub>N</sub>	r <sub>N</sub>	H <sub>L</sub>	slope <sub>A2</sub>	slope <sub>T</sub>				f <sub>T</sub>	r <sub>T</sub>
Lava sequence in Raiatea Island (16.849°S, 151.370°W)																		
RT05-06-1(T)	43.2	337	2.056	0.1975	10.7	20	0.541	0.261	0.447	0.995	0	1.01	0.970	0.999	0.999	20.0	5.22	23.5
RT06-01-2w	61.0	256			0.8	22	1.02	0.241	0.863	0.996	38	1.05	1.02	0.996	0.999	10.0	2.41	15.2
RT07-01-2	48.1	155	2.011	0.2475	13.6	12	0.352	0.231	0.849	0.902	0	1.00	0.974	1.00	0.987	10.0		-0.4
RT07-05-2	25.6	124			19.4	12	0.579	0.244	0.530	0.997	14	0.995	1.04	0.713	0.997	10.0	2.44	-1.7
RT10-01-2w(T)	73.7	457	1.837	0.3167	9.1	15	0.318	0.384	0.515	0.995	0	0.991	1.01	1.01	0.999	10.0	3.84	15.6
RT10-01-3(T)	24.9	409	1.837	0.3167	9.9	15	0.341	0.288	0.492	0.975	5	0.992	1.04	0.952	0.998	10.0		9.2
RT10-02-1(T)	32.7	409			14.5	10	0.455	0.255	0.661	0.980	0	1.02	1.06	0.998	0.998	10.0		21.3
RT10-03-1(T)	104	434	1.648	0.2840	9.1	25	0.247	0.528	0.244	0.995	0	1.03	0.956	1.02	0.997	10.0	5.28	7.2
RT10-03-2(T)	41.7	424	1.648	0.2840	9.1	15	0.334	0.307	0.516	0.995	0	0.993	1.03	1.00	0.996	10.0	3.07	3.2
RT11-01-2	26.7	111	1.709	0.2393	12.0	12	1.04	0.238	0.950	0.995	0	0.995	1.01	0.999	0.999	10.0	2.38	0.9
RT11-02-2	32.2	115			11.3	18	1.17	0.281	0.827	0.995	0	0.994	1.02	1.00	0.997	10.0	2.81	-1.1
RT11-04-3	45.6	163			-0.2	18	1.28	0.302	0.809	0.996	0	0.989	1.04	0.999	1.00	10.0	3.02	13.0
RT11-06-1	42.5	159			12.0	10	0.635	0.292	0.883	0.996	0	1.01	0.987	1.00	0.998	10.0	2.92	1.7
RT11-07-2	50.4	183	1.632	0.2779	10.7	10	0.607	0.310	0.687	0.995	0	0.973	1.05	0.999	0.999	10.0	3.10	2.9
RT11-11-1m	72.9	165			5.7	16	0.453	0.522	0.688	0.995	0	0.993	1.03	0.994	0.998	10.0	5.22	3.2

NRM<sub>0</sub>, ARM0<sub>0</sub>, initial NRM and ARM0 intensity after LTD (10<sup>-5</sup> Am<sup>2</sup>/kg); LTD, LT demagnetized fraction of ARM0 (per cent); H<sub>L</sub>, the lowest coercivity force taken for the linear segments; slope<sub>A1</sub>, slope<sub>A2</sub>, slopes of ARM spectra (≥ H<sub>L</sub>) in the ARM0-ARM1 and ARM1-ARM2 diagrams; slope<sub>N</sub>, slope<sub>T</sub>, slopes of the linear segments in the NRM-TRM1\* and TRM1-TRM2\* diagrams; f<sub>N</sub>, f<sub>T</sub>, NRM and TRM1 fractions of the linear NRM-TRM1\* and TRM1-TRM2\* segments; r<sub>N</sub>, r<sub>T</sub>, correlation coefficients of the linear NRM-TRM1\* and TRM1-TRM2\* segments; F<sub>L</sub>, laboratory induced DC field for TRM1 and TRM2; F, calculated palaeointensity; ΔAIC, AIC difference between linear and quadratic fit (Yamamoto & Tsunakawa 2005). Results are listed from top (RT05) to bottom (RT11) of the lava sequence. Parentheses with ‘T’ indicate that the specimens were measured previously at the Tokyo Institute of Technology (Yamamoto & Tsunakawa 2005). Numbers in italic indicate out of the selection criteria. Note that palaeointensities from specimens with suffix ‘w’ and ‘m’ are calculated with corrections for mass changes and excluded as outliers in the calculation of the flow average, respectively.

**Table 4.** Results of the LTD-DHT Shaw palaeointensities for the Tahaa samples.

Sample ID	NRM <sub>0</sub>	ARM <sub>0</sub>	B <sub>rc</sub> /B <sub>c</sub>	M <sub>rs</sub> /M <sub>s</sub>	LTD (per cent)	First heating						Second heating						F <sub>L</sub> (μT)	F (μT)	ΔAIC
						H <sub>L</sub>	slope <sub>A1</sub>	slope <sub>N</sub>	f <sub>N</sub>	r <sub>N</sub>	H <sub>L</sub>	slope <sub>A2</sub>	slope <sub>T</sub>	f <sub>T</sub>	r <sub>T</sub>					
Lava sequence in Tahaa Island (16.677°S, 151.454°W)																				
TA07-01-3	28.4	62.4			11.6	12	0.985	0.352	0.788	0.995	0	0.985	0.967	1.01	0.999	10.0	3.52	18.6		
TA07-03-2	22.4	64.0	2.238	0.1710	8.4	12	1.10	0.314	0.806	0.995	0	0.994	0.990	0.992	0.999	10.0	3.14	6.0		
TA07-06-3	30.6	63.5			9.6	10	1.10	0.354	0.758	0.995	0	0.980	0.982	0.984	0.999	10.0	3.54	-2.0		
TA07-07-1(T)	35.0	128			13.0	15	1.10	0.223	0.714	0.996	0	1.00	0.973	0.989	0.999	20.0	4.46	9.3		
TA06-01-2	39.8	93.3			15.9	20	0.751	0.438	0.560	0.996	0	0.992	1.05	0.988	0.998	10.0	4.38	4.1		
TA06-02-2	40.9	100	1.738	0.2467	10.9	16	0.741	0.408	0.708	0.998	0	1.00	1.03	0.985	0.998	10.0	4.08	-0.9		
TA06-03-1	41.3	98.1			11.3	16	0.786	0.412	0.682	0.995	0	0.997	1.03	0.984	0.997	10.0	4.12	5.9		
TA06-04-2	34.7	86.9			12.9	20	0.737	0.442	0.572	0.995	0	0.999	1.01	0.980	0.998	10.0	4.42	16.3		
TA06-05-2	57.5	126			11.7	16	0.552	0.376	0.500	0.970	0	1.01	1.04	0.991	0.998	10.0	4.42	-1.6		
TA06-06-2	44.5	111			12.2	14	0.737	0.383	0.679	0.994	0	0.996	1.08	0.995	0.999	10.0	3.69	-0.9		
TA06-07-2	34.7	98.4			8.2	16	0.827	0.369	0.711	0.997	0	0.983	1.05	0.972	0.999	10.0	3.69	-2.0		
TA06-12-1	38.8	104			9.7	10	0.816	0.339	0.797	0.996	0	0.992	1.06	0.996	0.999	10.0	3.69	-1.9		
TA05-01-2	50.8	155			9.4	8	0.906	0.325	0.954	0.998	0	1.02	1.03	0.991	1.00	10.0	3.25	0.1		
TA05-02-2	50.4	156			10.2	8	0.937	0.314	0.964	0.997	0	1.04	1.05	0.995	0.998	10.0	3.14	-1.3		
TA05-03-3	48.0	150	1.701	0.3150	9.3	4	0.937	0.313	0.988	0.999	0	1.02	1.02	0.995	0.998	10.0	3.13	0.9		
TA05-04-4	45.9	159			7.4	8	0.979	0.312	0.953	0.995	0	1.04	1.03	1.01	0.999	10.0	3.12	5.5		
TA04-01-1(T)	84.2	486			10.7	20	0.334	0.145	0.301	0.995	20	0.990	0.986	0.677	0.995	20.0	2.90	-1.6		
TA04-02-2	34.6	250			9.1	10	0.425	0.172	0.516	0.999	12	1.12	1.03	0.801	0.996	10.0	1.72	-1.9		
TA04-03-3	32.3	156	1.763	0.2053	13.9	14	0.495	0.389	0.589	0.995	0	1.03	0.953	0.965	0.998	10.0	3.89	5.1		
TA04-04-3	31.1	223			9.3	8	0.529	0.279	0.548	0.978	0	1.02	1.09	0.971	0.997	10.0	6.5	6.5		
TA04-05-2	309	238			12.7	8	0.260	0.303	0.389	0.931	0	0.986	1.07	1.02	0.998	10.0	1.7	1.7		
TA04-07-2	359	249			12.6	8	0.343	0.201	0.501	0.880	0	1.00	1.11	0.983	0.992	10.0	7.5	7.5		
TA04-08-1(T)	61.5	324			18.0	10	0.480	0.555	0.631	0.980	0	1.04	0.979	0.997	0.997	10.0	18.9	18.9		

Results are listed from top (TA07) to bottom (TA04) of the lava sequence.

Table 5. Results of the LTD-DHT Shaw palaeointensities for the Maupiti samples.

Sample ID	NRM <sub>0</sub>	ARM <sub>0</sub>	B <sub>rc</sub> /B <sub>c</sub>	M <sub>rs</sub> /M <sub>s</sub>	LTD (per cent)	First heating				Second heating				F <sub>L</sub> (μT)	F (μT)	ΔAIC		
						H <sub>L</sub>	slope <sub>A1</sub>	slope <sub>N</sub>	f <sub>N</sub>	r <sub>N</sub>	H <sub>L</sub>	slope <sub>A2</sub>	slope <sub>T</sub>				f <sub>T</sub>	r <sub>T</sub>
Dyke in Maupiti Island (16.438°S, 152.253°W)																		
MP01-02-1(T)	15.9	138	2.100	0.2484	8.3	20	1.45	0.419	0.816	0.995	0	0.937	1.02	0.971	0.995	10.0	4.19	-1.8
MP01-03-1	16.5	70.2	2.240	0.2178	7.2	22	1.14	0.495	0.674	0.995	4	0.880	1.03	0.957	0.996	10.0	4.95	-0.3
MP01-04-1(T)	16.7	154			8.3	30	1.26	0.425	0.501	0.995	5	0.878	0.997	0.849	0.997	10.0	4.25	-2.0
MP01-05-1	20.5	57.6			17.4	18	0.553	0.535	0.358	0.997	12	0.899	0.987	0.863	0.997	10.0	5.35	-1.6
MP01-06-1(T)	21.3	126			16.7	25	0.573	0.466	0.456	0.990	5	0.823	1.20	0.690	0.987	10.0		3.7
MP01-07-1(T)	14.5	134			16.7	30	0.919	0.375	0.394	0.995	5	0.893	1.04	0.777	0.996	10.0	3.75	-1.9
MP01-08-1	13.8	51.8			27.1	20	0.507	0.439	0.332	0.995	4	0.958	0.988	0.923	0.996	10.0	4.39	0.3
MP01-09-1(T)	12.2	108			25.4	20	0.426	0.410	0.367	0.983	0	1.00	0.978	0.997	0.993	10.0		-0.1
MP01-12-1(T)	18.3	124			14.5	30	0.607	0.465	0.327	0.995	0	0.906	1.01	0.968	0.996	10.0	4.65	-1.3

samples plotting in the upper-left region along the mixing curves (e.g. Fig. 4a) considered to have a higher oxidation state than those plotting in the lower-right region (e.g. Fig. 4f).

Low-field susceptibilities of powdered fractions from six palaeomagnetic cores were measured using a KLY-4S Kappabridge with a CS-3 furnace apparatus (AGICO) over the temperature range of 30 to 700 °C. The measurements were performed in continuous argon gas flow with a field of 300 A m<sup>-1</sup> (~0.4 mT) and an operating frequency of 875 Hz. The results are illustrated in Fig. 5. In the heating curves, main peaks are recognized at 450–550 °C. Since these peaks correspond approximately to the Curie temperature (*T<sub>c</sub>*) of the main magnetic phase, the main magnetic carriers of the present samples are estimated to be Ti-poor titanomagnetites of ~TM05-TM20 probably originating from deuteric oxidation of low-Ti TM grains. This is consistent with the hysteresis interpretations from the Day plot.

In summary, the main remanence carriers in the samples studied are Ti-poor TMs (TM05-TM20) with a relatively large contribution of SD-like components, probably originating from deuteric oxidation of low-Ti TM grains. Considering previous studies using historical lava flows (Yamamoto *et al.* 2003; Mochizuki *et al.* 2004; Oishi *et al.* 2005), the present samples seem to be suited for the LTD-DHT Shaw palaeointensity experiment.

#### 4.2 Palaeodirection

Stepwise thermal demagnetization (ThD) and alternating field demagnetization (AFD) were previously conducted on at least two specimens from each site (total 65 specimens; Yamamoto *et al.* 2002). Further AFD was carried out on 40 specimens as part of the LTD-DHT Shaw experiment in Yamamoto & Tsunakawa (2005), and the present study. We report all these results together.

After removal of secondary components by about 425 °C or 25 mT, most of the demagnetization results yielded primary components with MAD (maximum angular deviation; Kirschvink 1980) ≤10.0° (Fig. 6). Some specimens from each site (except for RT05, RT06 and TA05) gave demagnetization vectors along great circle paths toward certain directions (Fig. 7). Because these directions are consistent with the stable primary directions determined from other specimens, mean palaeomagnetic directions were determined by analysing the stable primary directions (e.g. Fig. 6) together with the best-fitting great circles (e.g. Fig. 7) following McFadden and McElhinny (1988). Results of statistical calculations are listed in Table 6.

The mean palaeomagnetic directions show good statistical quality ( $\alpha_{95} < 8.0^\circ$ ) for all sites apart from RT04 and even for RT04, with  $\alpha_{95} = 15.0^\circ$  this is considered to be acceptable. The corresponding VGP latitudes range between 0.7°N and 52.4°N, indicating a transitional geomagnetic field.

#### 4.3 Palaeointensity

In the present study, 32 samples (nine from Raiatea, twenty from Tahaa and three from Maupiti Island) were measured using the LTD-DHT Shaw method (Tsunakawa *et al.* 1997; Yamamoto *et al.* 2003) at the Geological Survey of Japan, AIST. 15 samples from these islands were previously measured at the Tokyo Institute of Technology (Yamamoto & Tsunakawa 2005), thus we report all these results together (total 47 results).

In the present experiment, a laboratory TRM was imparted by heating the samples in vacuum (10–10<sup>2</sup> Pa) at a top temperature of

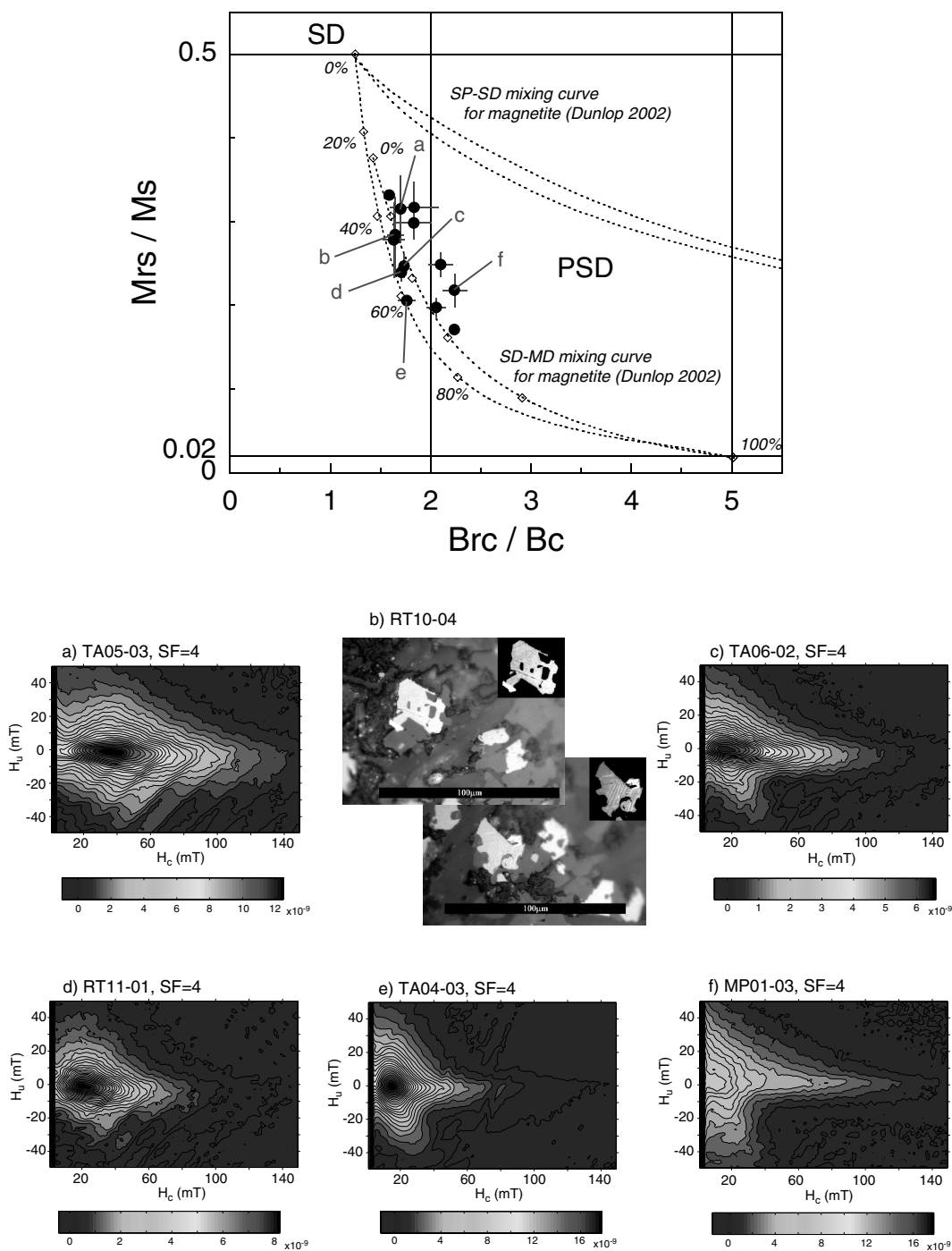


**Figure 4.** Day plot (Day *et al.* 1977) for the core-averaged hysteresis parameters of 14 selected palaeomagnetic cores. Each data point is associated with error bars (one standard deviation). Some threshold values are modified following Dunlop (2002). Numbers along the mixing curves (Dunlop 2002) indicate per cent of MD components. FORC diagrams (samples labelled a, c, d, e and f) and the photographs under reflected light (sample b) are also shown.

610 °C for 24 (first heating) and 48 min (second heating) in a DC field (10.0–20.0  $\mu\text{T}$ ). Anhyseretic remanent magnetization (ARM) was given by a 50  $\mu\text{T}$  biasing field with a smoothly decreasing AF field of 180 mT. The samples were subjected to progressive AF demagnetization at 2–10 mT intervals up to 180 mT. All remanences were measured with an automatic spinner magnetometer with AF demagnetizer (Natsuhara-Giken Dspin-2: Kono *et al.* 1984, 1997). Prior to progressive AF demagnetization of NRM, TRM and ARM, specimens were soaked in liquid nitrogen for 10 min and then kept

at room temperature for an hour to conduct the low temperature demagnetization (LTD; Ozima *et al.* 1964; Heider *et al.* 1992). The liquid nitrogen was in a plastic dewar and the complete cycle carried out in a magnetically shielded case. The details of the experimental procedures are described in Yamamoto *et al.* (2003) and Yamamoto & Tsunakawa (2005).

NRM-TRM1\* and TRM1-TRM2\* diagrams were constructed from the experimental results where TRM1\* and TRM2\* denote TRM1 and TRM2 corrected using the technique of Rolph & Shaw

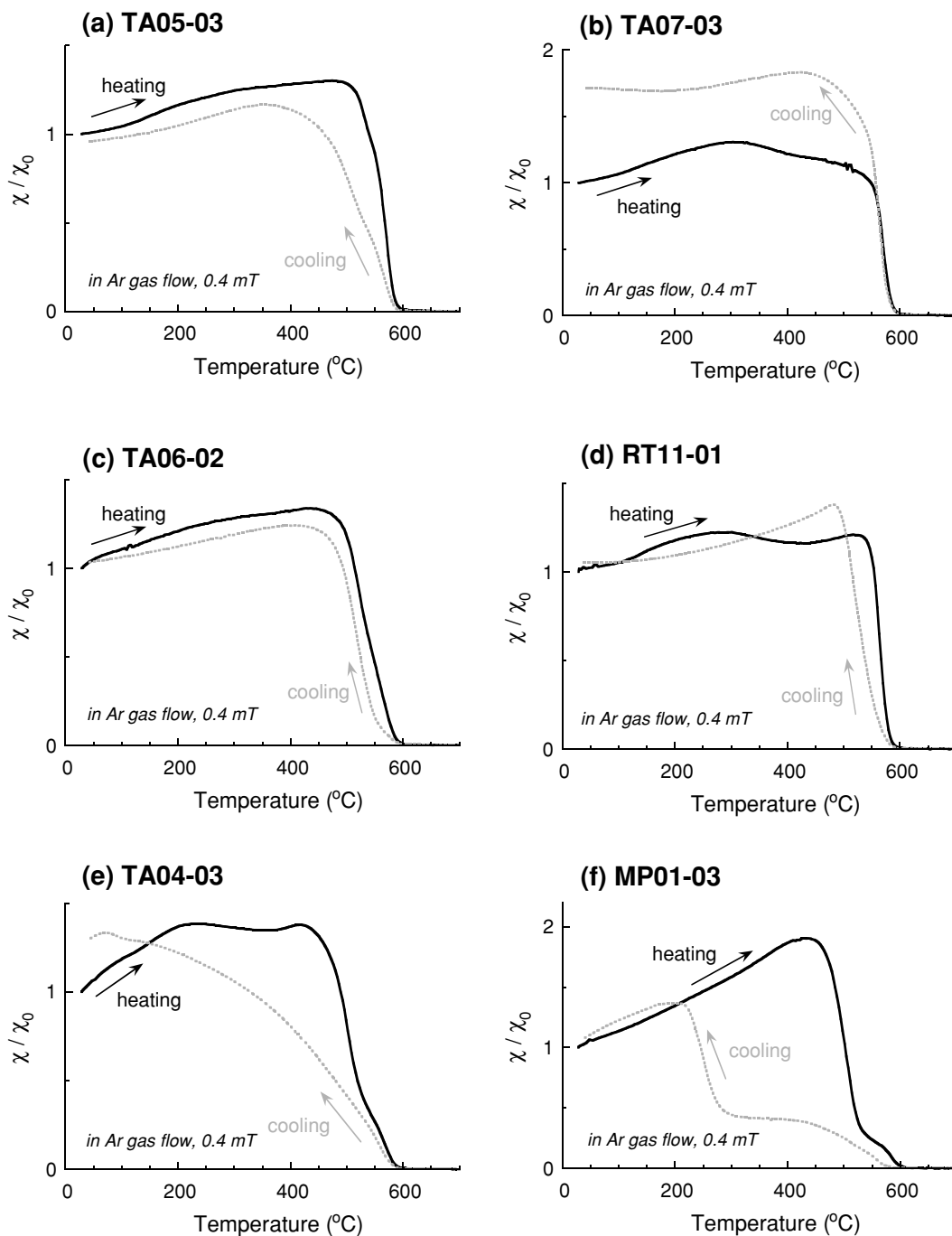


**Figure 5.** Temperature dependent magnetic susceptibility curves for the samples from six sites. The measurements were performed with continuous argon gas flow, under the field of  $300 \text{ A m}^{-1}$  ( $\sim 0.4 \text{ mT}$ ,  $875 \text{ Hz}$ ). Note that the susceptibilities ( $\chi$ ) are normalized by the room temperature values ( $\chi_0$ ).

(1985). These corrections are based on an assumption that changes in the coercivity spectra of TRM can be followed by those of ARM. Similar to previous studies (Yamamoto *et al.* 2003; Mochizuki *et al.* 2004; Oishi *et al.* 2005; Yamamoto & Tsunakawa 2005; Mochizuki *et al.* 2006), the results are judged by the following quantitative selection criteria.

- (1) A stable primary component of remanence is recognized in the orthogonal plot obtained from AF demagnetization of the NRM.
- (2) A linear portion should exist in the NRM-TRM1\* diagram which is not less than 15 per cent of the original NRM intensity

( $f_N \geq 0.15$ ), and the correlation coefficient should be larger than 0.995 ( $r_N \geq 0.995$ ).

- (3) The linear portion ( $f_T \geq 0.15$  and  $r_T \geq 0.995$ ) should also exist in the TRM1 - TRM2\* diagram. The slope must be unity within experimental errors ( $1.05 \geq \text{Slope}_T \geq 0.95$ ) as a proof of the validity of the ARM correction.

For a schematic view of the data analysis, the reader is referred to Fig. 6 of Yamamoto & Tsunakawa (2005).

On application of the selection criteria, 35 successful results were obtained (12, 16 and 7 results for Raiatea, Tahaa and Maupiti,

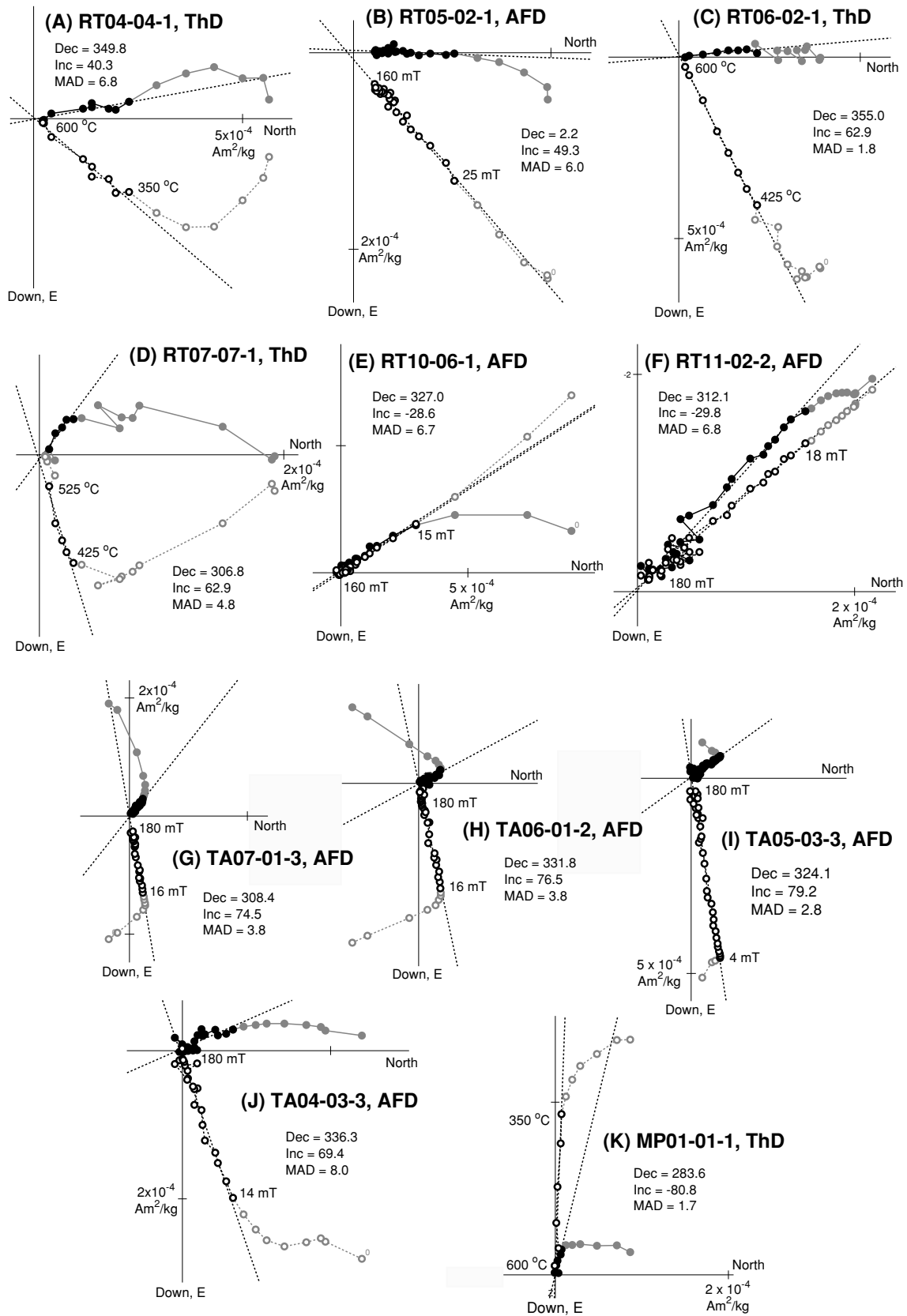
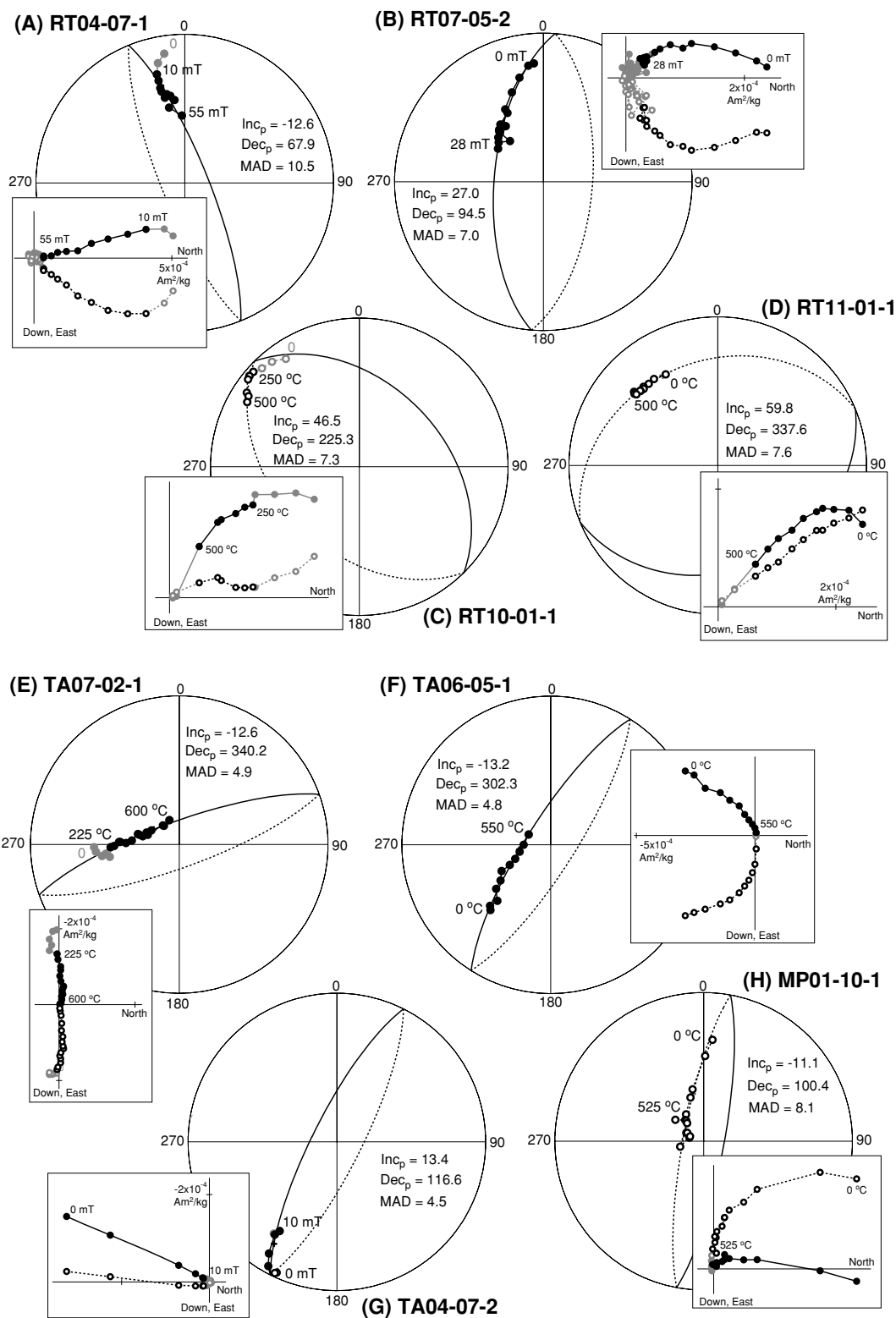


Figure 6. Representative orthogonal vector plots of ThD or AFD from each site. Closed and open circles indicate horizontal and vertical projections, respectively.



**Figure 7.** Examples of demagnetization behaviours trending great circles. These behaviours are observed from some samples from each site except for RT05, RT06 and TA05. In each figure, inclination ( $Inc_p$ ), declination ( $Dec_p$ ) and maximum angular deviation ( $MAD$ ) of a best-fitting great circle are indicated.

respectively). Representative diagrams are shown in Fig. 8 and all individual results are summarized in Tables 3–5. Note that the 15 results previously obtained were reanalysed in this study. Unsuccessful results were rejected mainly due to low correlation coefficients

in the NRM-TRM1\* diagrams ( $r_N < 0.995$ ). Readers may feel that the criterion of (2) is not stringent, but 80 per cent of the successful results gave  $f_N$  values larger than 0.50.  $\Delta AIC$  values, which are measure of the preferences between the linear and quadratic fits in

**Table 6.** Statistical results of the palaeodirections and the LTD-DHT Shaw palaeointensities.

Site	$N_d$	Dec (°)	Inc (°)	$\alpha_{95}$ (°)	$P_{Lat}$ (°)	$P_{Long}$ (°)	$N_F$	F ( $\mu$ T)	VDM ( $10^{22}$ A m <sup>2</sup> )	VADM ( $10^{22}$ A m <sup>2</sup> )	$\Delta AIC_{min}$
lava sequence in Raiatea Island (16.849°S, 151.370°W)											
RT04	7	351.1	41.1	15.0	48.7	-163.8	0				
RT05	6	2.1	51.1	3.2	41.3	-149.0	1	5.22	1.00	1.21	23.5
RT06	8	356.1	59.6	2.6	32.6	-154.9	1	2.41	0.416	0.559	15.2
RT07	8	308.5	62.9	5.9	12.9	-186.4	1	2.44	0.403	0.566	-1.7
RT10	8	316.9	-25.2	8.0	48.3	117.5	3	<i>4.06 ± 1.12</i>	<i>0.980</i>	<i>0.942</i>	3.2
RT11m	9	321.1	-26.2	4.6	52.4	117.7	5	2.85 ± 0.28	0.682	0.660	-1.1
lava sequence in Tahaa Island (16.677°S, 151.454°W)											
TA07	8	301.7	68.8	5.0	4.7	-183.0	4	3.67 ± 0.56	0.554	0.851	-2.0
TA06	10	324.3	74.4	1.8	7.4	-168.1	5	4.14 ± 0.29	0.592	0.961	-2.0
TA05	11	323.2	78.9	2.9	0.7	-164.1	4	3.16 ± 0.06	0.433	0.734	-1.3
TA04	8	339.9	69.7	3.3	17.7	-163.8	3	<i>2.84 ± 1.09</i>	<i>0.443</i>	<i>0.659</i>	-1.9
dyke in Maupiti Island (16.438°S, 152.253°W)											
MP01	11	297.9	-77.8	2.1	26.0	50.7	7	4.50 ± 0.53	0.650	1.049	-2.0

Site, site ID;  $N_d$ , number of the specimens used for the calculation of palaeodirection; Dec, Inc,  $\alpha_{95}$ , palaeodirection and its 95 per cent confidence circle;  $P_{Lat}$ ,  $P_{Long}$ , latitude and longitude of the virtual geomagnetic pole;  $N_F$ , number of the specimens used for the calculation of mean palaeointensity;  $F$ , mean palaeointensity with its standard deviation; VDM, VADM, virtual dipole moment and virtual axial dipole moment;  $\Delta AIC_{min}$ , minimum AIC values for the individual sites. Note that the mean palaeointensity is calculated without the outliers (multispesimen test) for the site ID with suffix of 'm'. Mean palaeointensities from RT10 and TA04 (in italic) are not considered to accurately represent the ancient geomagnetic field because they resulted in standard deviations exceeding 20 per cent (see text).

the NRM-TRM1\* diagrams (Yamamoto & Tsunakawa 2005), resulted in the values less than 15.0 for 86 per cent of the successful results. Because the previous LTD-DHT Shaw experiments on the Society samples suggest that  $\Delta AIC$  exceeding  $\sim 15$  is possibly a sign of an undesirable palaeointensity (Yamamoto & Tsunakawa 2005), the present results are considered to have good quality. Resultant palaeointensity ranges between 1.72 and 5.28  $\mu$ T, which is less than about 15 per cent of the present field value (34.3  $\mu$ T at the sampling location; IGRF-10 model, IAGA Division V Working Group VMOD 2005).

From statistical calculations of multiple results from the same cooling unit, experiments using historical lava flows indicate that the precision of the LTD-DHT Shaw method is about 10 per cent (Yamamoto *et al.* 2003; Mochizuki *et al.* 2004; Oishi *et al.* 2005). The precision may be expected to be less for older volcanic rocks as they are not so ideal for palaeointensity study (e.g. may have undergone a certain amount of weathering) in which case we deem within flow variability of 20 per cent as acceptable. We require at least three successful results for each cooling unit to be able to provide a meaningful estimate of the ancient geomagnetic field. In the present study (Table 6), seven sites (RT10, RT11, TA04, TA05, TA06, TA07 and MP01) fulfil this condition. However, mean palaeointensities from two of these sites (RT10 and TA04) resulted in standard deviations exceeding 20 per cent and are thus not considered to accurately represent the ancient geomagnetic field. If we exclude these data, VDMs (virtual dipole moments) from the remaining five sites range between 0.433 and  $0.682 \times 10^{22}$  A m<sup>2</sup>.

## 5 DISCUSSION

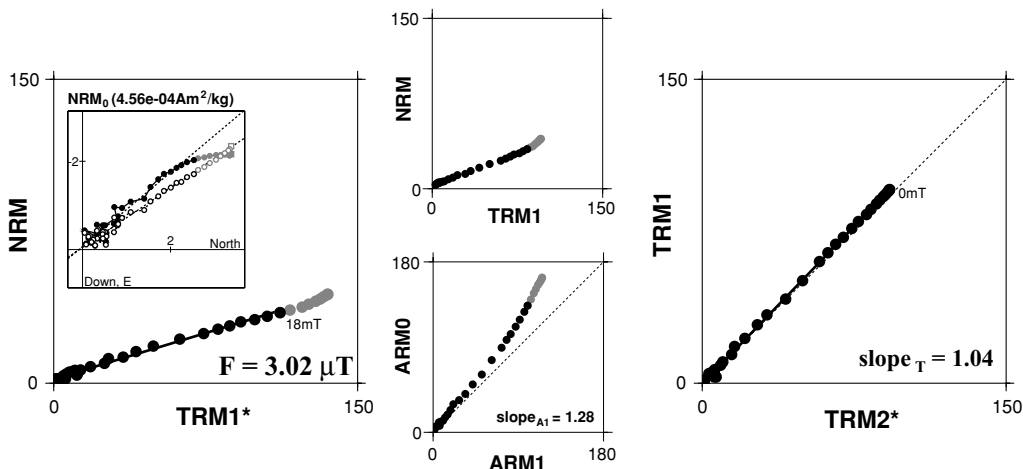
Low VGP latitudes (e.g.  $< 45^\circ$ ; Verosub & Banerjee 1977) and low VDM values (e.g.  $< 2 \times 10^{22}$  Am<sup>2</sup>; Mochizuki *et al.* 2006) are typical characteristics of the transitional geomagnetic field. As the samples from this study resulted in VGP latitudes of 0.7–52.4°N and VDM values of 0.433–0.682  $\times 10^{22}$  A m<sup>2</sup>, they are considered to record the transitional field. The timing of these events are  $2.77 \pm$

0.02 Ma (Raiatea),  $3.20 \pm 0.03$  Ma (Tahaa) and  $4.40 \pm 0.01$  Ma (Maupiti) from the <sup>40</sup>Ar/<sup>39</sup>Ar dating results.

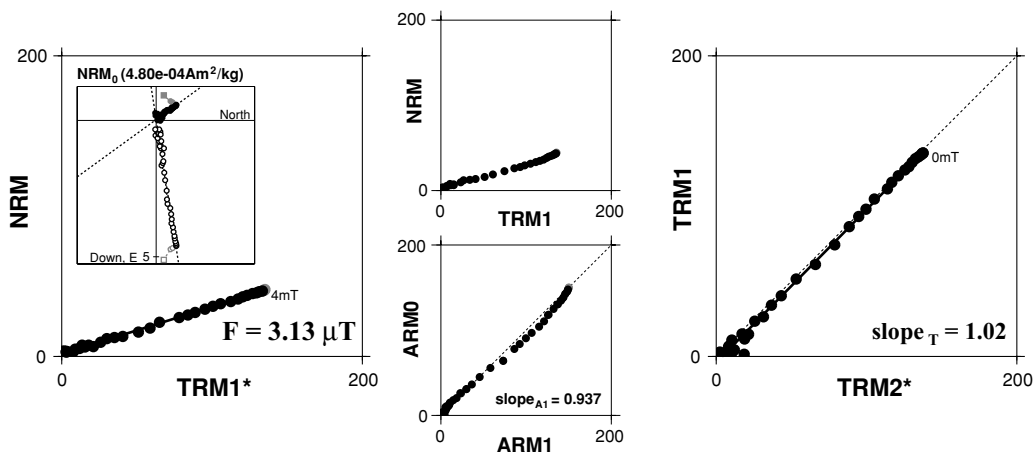
In order to see if the events recorded in the Society Islands samples correspond to unknown geomagnetic excursions, it is necessary to compare their ages with the existing GPTS. The GPTS by Cande & Kent (1995) is widely accepted as a definitive chronology for the late Cretaceous and Cenozoic. It has been constructed from marine magnetic anomalies from the world's ocean basins with mostly radioisotopically dated calibration points. However, in this GPTS, subchrons younger than 5.23 Ma were directly inserted from the astrochronology of Shackleton *et al.* (1990) and Hilgen (1991), with a refined astronomical age suggested for the Matuyama-Gauss boundary by Langereis *et al.* (1994). For the Pliocene and Pleistocene, the GPTS by Cande & Kent (1995) is equivalent to the astronomical polarity timescale (APTS). The APTS is obtained by using the periodic character of Milankovitch cycles as a precise dating tool. Strictly speaking, it is not considered valid to compare our data directly with this GPTS because the radioisotopic dating has a different physical background compared with the astronomical calibration. However, many studies (e.g. McDougall *et al.* 1992; Baksi 1995; Horg *et al.* 2002) have confirmed a consistency in age between radioisotopically and astronomically calibrated GPTSs for younger periods, though it has not yet been systematically examined for the Pliocene and Pleistocene.

Comparison with the GPTS suggests that the two events at  $3.20 \pm 0.03$  Ma (Tahaa) and  $4.40 \pm 0.01$  Ma (Maupiti) probably correspond to known polarity transitions (Fig. 9). Radioisotopic measurements on terrestrial materials from the literature report the upper boundary age of the Mammoth reversed subchron as  $3.21 \pm 0.06$  Ma (McDougall *et al.* 1992),  $3.17 \pm 0.01$  Ma (Renne *et al.* 1993) and 3.17 Ma (Baksi 1995). The upper boundary for the Nunivak normal subchron is suggested to be 4.42 Ma (Baksi 1995), 4.43 Ma (Clement *et al.* 1997) and  $4.449 \pm 0.087$  Ma (Renne *et al.* 1999). These ages are indistinguishable from the present <sup>40</sup>Ar/<sup>39</sup>Ar ages (note that reported <sup>40</sup>Ar/<sup>39</sup>Ar ages are recalculated relative to 27.5 Ma FCTS). It is natural to consider that the two events originate from these polarity transitions.

**(A) RT11-04-3**



**(B) TA05-03-3**



**(C) MP01-03-1**

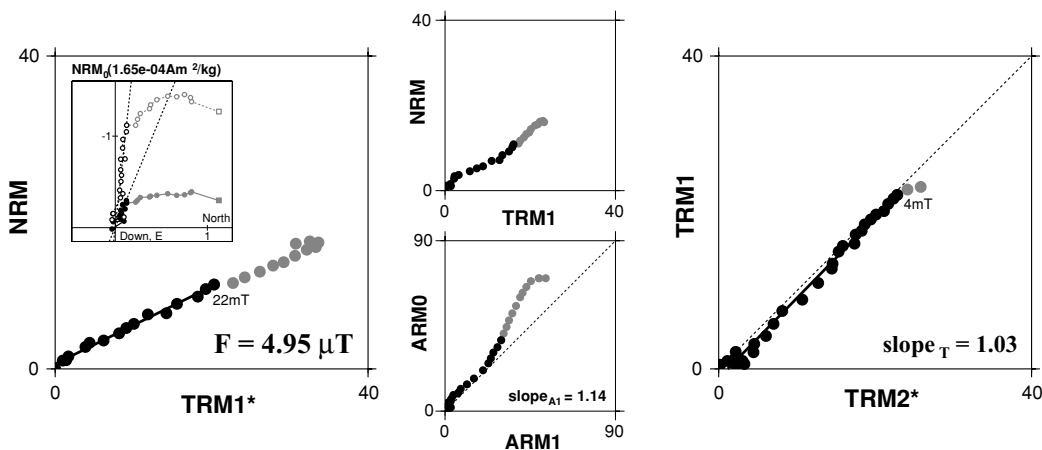


**Figure 8.** Representative successful LTD-DHT Shaw palaeointensity results. (a) RT11-04-3, (b) TA05-03-3 and (c) MP01-03-1. The left three diagrams illustrate results from the first laboratory heating while the right one is from the second heating. Linear portions consist of closed symbols. Orthogonal vector plots of AFD on NRM are also shown as insets, where closed and open symbols indicate projections onto horizontal and vertical planes, respectively (squares are NRM before LTD). Units are in  $10^{-5} \text{ A m}^2 \text{ kg}^{-1}$ .

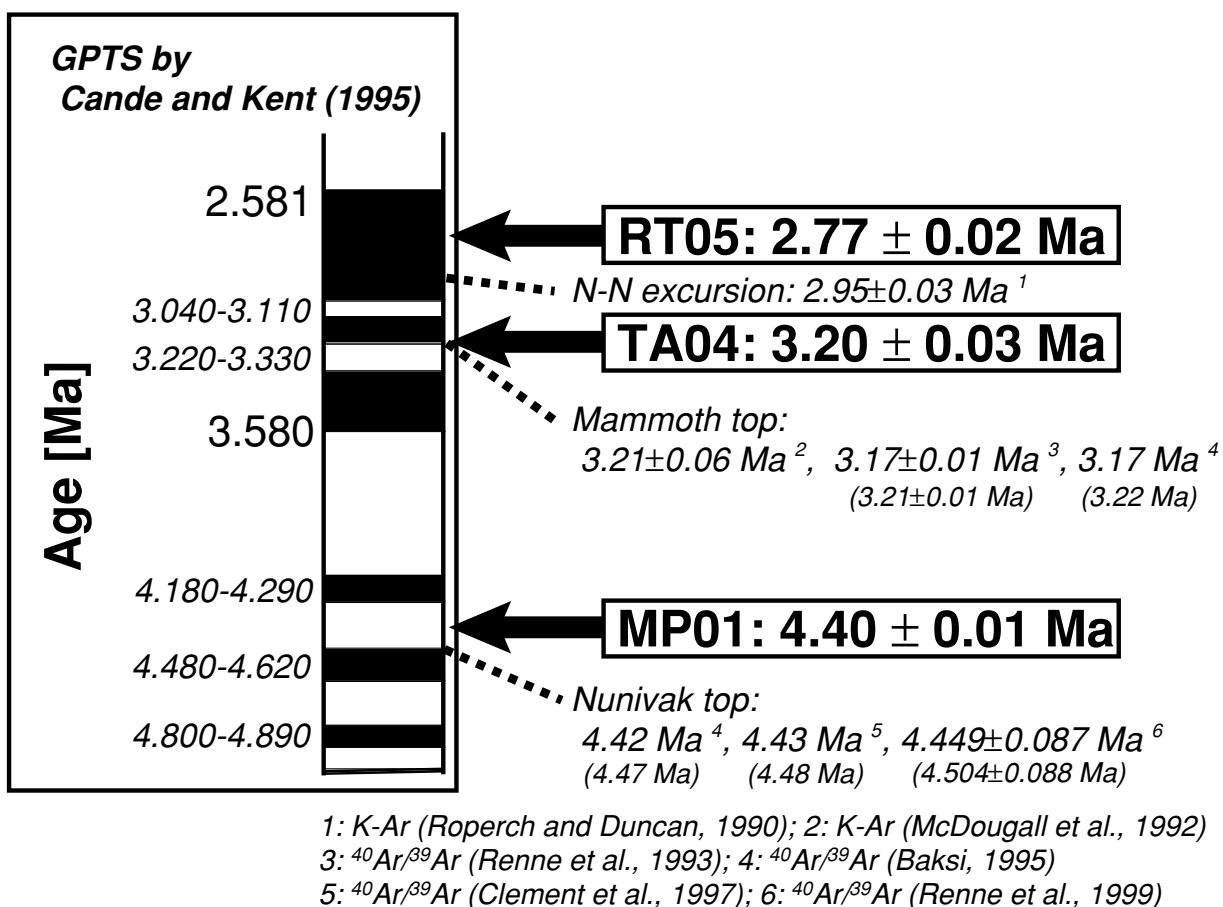


**Figure 9.** Comparison between the present results with the reported GPTS.  $^{40}\text{Ar}/^{39}\text{Ar}$  ages are recalculated relative to 27.5 Ma FCTS, and original values are indicated in parentheses (if recalculations were made). The geomagnetic event at  $2.77 \pm 0.02$  Ma (RT05) might be a previously unknown geomagnetic excursion (Raiatea excursion) while those at  $3.20 \pm 0.03$  Ma (TA04) and  $4.40 \pm 0.01$  Ma (MP01) probably correspond to the upper boundary ages of the Mammoth reversed subchron and the Nunivak normal subchron.

The event at  $2.77 \pm 0.02$  Ma (Raiatea) does not correspond to any known polarity transitions, and therefore, might be a record of a previously unknown geomagnetic excursion. There are no known polarity transitions in the vicinity of this age (Fig. 9). Roperch & Duncan (1990) reported an apparent N-N excursion from volcanic rocks on the Huahine Island, but the evaluated K-Ar age of  $2.95 \pm 0.03$  Ma (weighted-average) for these volcanic rocks is significantly different from the present  $^{40}\text{Ar}/^{39}\text{Ar}$  age. In the relative palaeointensity stack of EPAPIS-3 Ma (0.8–3.0 Ma; Yamazaki & Oda 2005), palaeointensity lows are recognized, both at  $\sim 2.77$  Ma and  $\sim 2.95$  Ma (Fig. 10). It is therefore, suggested that the Raiatea record probably corresponds to an unknown geomagnetic excursion posterior to that reported by Roperch & Duncan (1990).

There has been a growing consensus that geomagnetic excursions are associated with relative palaeointensity lows (e.g. Oda 2005). The idea has also been supported from absolute palaeointensities from terrestrial materials (e.g. Mochizuki et al. 2006). In the EPAPIS-3 Ma curve (Yamazaki & Oda 2005), there are many other relative palaeointensity lows which have not yet been correlated with geomagnetic excursions. Geomagnetic excursions are probably recurrent not only in the Brunhes Chron but also in the Matuyama and upper-Gauss Chrons.

## 6 CONCLUSION

The present  $^{40}\text{Ar}/^{39}\text{Ar}$  dating and palaeomagnetic measurements revealed that the geomagnetic field was in transitional state at  $2.77 \pm 0.02$ ,  $3.20 \pm 0.03$  and  $4.40 \pm 0.01$  Ma, at least in the vicinity of the Society Islands. Considering the reported radioisotopic ages for geomagnetic events, the first event might be an unknown geomagnetic excursion (Raiatea excursion) whilst the latter two probably correspond to known polarity transitions (upper boundary ages of the Mammoth reversed subchron and the Nunivak normal subchron). The existence of the Raiatea excursion is supported from the contemporaneous palaeointensity low recognized in the relative palaeointensity stack (EPAPIS-3 Ma; Yamazaki and Oda, 2005). Geomagnetic excursions are probably recurrent not only in the Brunhes Chron but also in the Matuyama and upper-Gauss Chrons.

## ACKNOWLEDGMENTS

We are grateful to Hideo Tsunakawa of Tokyo Institute of Technology and Toshitsugu Yamazaki of Geological Survey of Japan, AIST, for use of rock magnetic and palaeomagnetic facilities. We thank Koichiro Shimura for help in thermal demagnetization

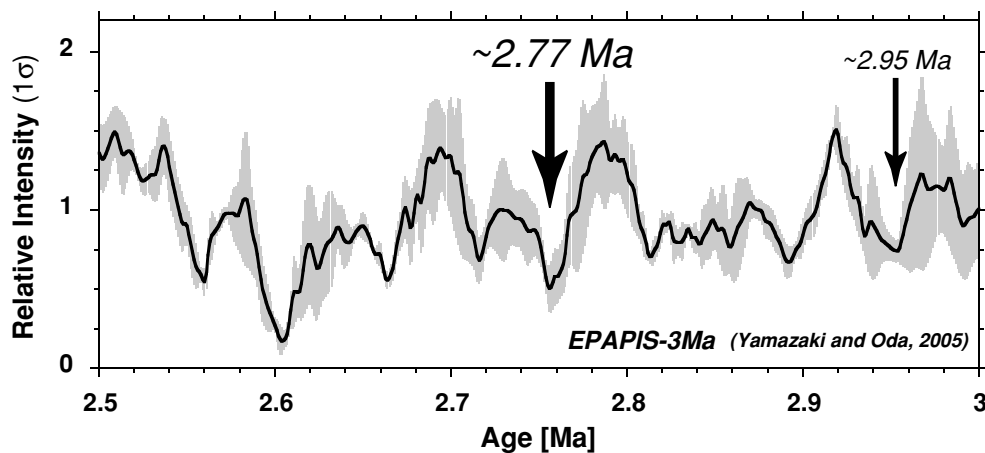


**Figure 10.** Relative palaeointensity variation during 2.5–3.0 Ma in the EPAPIS-3 Ma curve (Yamazaki & Oda 2005). Palaeointensity lows are recognized at  $\sim 2.77$  and  $\sim 2.95$  Ma.

experiment. Akikazu Matsumoto of Geological Survey of Japan, AIST, is acknowledged for thorough help and suggestions in the  $^{40}\text{Ar}/^{39}\text{Ar}$  dating experiment. We appreciate the JMTR reactor for providing opportunity to irradiate samples for  $^{40}\text{Ar}/^{39}\text{Ar}$  dating. FORC diagrams were drawn by the FORCAM program written by Michael Winklhofer, and palaeodirections were analysed by software offered by Hideo Tanaka of Kochi University. Constructive comments by Mimi Hill greatly improved the manuscript, and the two referees are thanked for the reviews. Y.Y. was supported from Research Fellowships of the Japan Society for the Promotion of Science for Young Scientists in the course of this study.

## REFERENCES

- Baksi, A.K., 1995. Fine tuning the radioisotopically derived geomagnetic polarity time scale (GPTS) for 0–10 Ma, *Geophys. Res. Lett.*, **22**, 457–460.
- Baksi, A.K., Hoffman, K.A. & McWilliams, M., 1993. Testing the accuracy of the geomagnetic polarity time-scale (GPTS) at 2–5 Ma, utilizing  $^{40}\text{Ar}/^{39}\text{Ar}$  incremental-heating data on whole-rock basalts, *Earth planet. Sci. Lett.*, **118**, 135–144.
- Binard, N., Hekinian, R., Cheminee, J.L., Searle, R.C. & Stoffers, P., 1991. Morphological and structural studies of the Society and Austral hotspot regions in the South Pacific, *Tectonophysics*, **186**, 293–312.
- Blais, S., Guille, G., Maury, R.C., Guillou, H., Miau, D. & Cotten, J., 1997. Geology and petrology of Raiatea Island (Society Islands, French Polynesia), *C. R. Acad. Sci. Paris, série IIA*, **324**, 435–442.
- Cande, S.C. & Kent, D.V., 1995. Revised calibration of the geomagnetic polarity timescale for the Late Cretaceous and Cenozoic, *J. geophys. Res.*, **100**, 6093–6095.
- Clement, B.M., Swisher, C.C. & Rodda, P., 1997. New magnetostratigraphic and  $^{40}\text{Ar}/^{39}\text{Ar}$  dating results from the Suva Marl, Fiji: Calibration of the Early Pliocene geomagnetic polarity time scale, *Earth planet. Sci. Lett.*, **151**, 107–115.
- Coe, R.S., Singer, B.S., Pringle, M.S. & Zhao, X., 2004. Matuyama-Brunhes reversal and Kamikatsura event on Maui: paleomagnetic directions,  $^{40}\text{Ar}/^{39}\text{Ar}$  ages and implications, *Earth planet. Sci. Lett.*, **222**, 667–684.
- Cox, A.V., 1968. Lengths of geomagnetic polarity intervals, *J. geophys. Res.*, **73**, 3247–3260.
- Dalrymple, G.B., Lanphere, L.A. & Clague, D.A., 1980. Conventional and  $^{40}\text{Ar}/^{39}\text{Ar}$  K-Ar ages of volcanic rocks from Ojin (Site 430), Nintoku (Site 483) seamounts and the chronology of volcanic propagation along the Hawaiian-Emperor chain, *Initial Rep. Deep Sea Drill. Proj.*, **55**, 54–76.
- Day, R., Fuller, M. & Schmidt, V.A., 1977. Hysteresis properties of titanomagnetites: grain-size and compositional dependence, *Phys. Earth planet. Int.*, **13**, 260–267.
- Diraison, C., 1991. Le volcanisme arien des archipels Polynesiens de la Societe, des Marquises et des Australes-Cook, *PhD thesis*, Universite de Bretagne Occidentale.
- Dunlop, D.J., 2002. Theory and application of the Day plot (Mrs/Ms versus Hcr/Hc) 1. Theoretical curves and tests using titanomagnetite data, *J. geophys. Res.*, **107**, 3, 10.1029/2001JB000486.
- Duncan, R.A. & McDougall, I., 1976. Linear volcanism in French Polynesia, *J. Volc. Geotherm. Res.*, **1**, 197–227.
- Fleck, R.J., Sutter, J.F. & Elliot, D.H., 1977. Interpretation of discordant  $^{40}\text{Ar}/^{39}\text{Ar}$  age-spectra of Mesozoic tholeiites from Antarctica, *Geochimica et Cosmochimica Acta*, **41**, 15–32.
- Guillou, H., Blais, S., Guille, G., Maury, R.C., Le Dez, A. & Cotten, J., 1998. Age (K-Ar) and duration of the subaerial build-up of Moorea, Raiatea and Maupiti (Society Islands, French Polynesia), *Geologie de la France*, **3**, 29–36.
- Heider, F., Dunlop, D.J. & Soffel, H.C., 1992. Low-temperature and alternating field demagnetization of saturation remanence and thermoremanence in magnetite grains (0.037  $\mu\text{m}$  to 5 mm), *J. geophys. Res.*, **97**, 9371–9381.
- Hilgen, F.J., 1991. Extension of the astronomically calibrated (polarity) time scale to the Miocene/Pliocene boundary, *Earth planet. Sci. Lett.*, **107**, 349–368.
- Horng, C.S., Lee, M.Y., Palike, H., Wei, K.Y., Liang, W.T., Iizuka, Y. & Torii, M., 2002. Astronomically calibrated ages for geomagnetic reversals within the Matuyama chron, *Earth Planets Space*, **54**, 679–690.
- Ishizuka, O., 1998. Vertical and horizontal variations of the fast neutron flux in a single irradiation capsule and their significance in the laser-heating  $^{40}\text{Ar}/^{39}\text{Ar}$  analysis: case study for the hydraulic rabbit facility of the JMTR reactor, Japan, *Geochem. J.*, **32**, 243–252.
- Ishizuka, O., Uto, K. & Yuasa, M., 2003. Volcanic history of the back-arc region of the Izu-Bonin (Ogasawara) arc, in *Intra-Oceanic Subduction Systems: Tectonic and Magmatic Processes*, pp. 187–205, eds Larter, R.D. & Leat, P.H., Geol. Soc. Spec. Publ.
- International Association of Geomagnetism and Aeronomy (IAGA), Division V, Working Group VMOD: Geomagnetic Field Modeling, 2005. The 10th-Generation International Geomagnetic Reference Field, *Geophys. J. Int.*, **161**, 561–565.
- Kirschvink J.L., 1980. The least-squares line and plane and the analysis of paleomagnetic data, *Geophys. J. R. astr. Soc.*, **62**, 699–718.
- Kono, M., Kitagawa, H. & Tanaka, H., 1997. Use of automatic spinner magnetometer—AF demagnetizer system for magnetostratigraphy and paleosecular variation studies (abstract), in *Proc. 8th Scientific Assembly IAGA, 1997 Abstract book*, pp. 66, Uppsala.

- Kono, M., Hamano, Y., Nishitani, T. & Tosha, T., 1984. A new spinner magnetometer: principles and techniques, *Geophys. J. R. astr. Soc.*, **67**, 217–227.
- Langerreis, G.G., Van Hoof, A.A.M. & Hilgen, F.J., 1994. Steadying the rates, *Nature*, **369**, 615.
- Lanphere, M.A. & Baadsgaard, H., 2001. Precise K-Ar,  $^{40}\text{Ar}/^{39}\text{Ar}$ , Rb-Sr and U/Pb mineral ages from the 27.5 Ma Fish Canyon Tuff reference standard, *Chem. Geol.*, **175**, 653–671.
- Lanphere, M.A. & Dalrymple, G.B., 1978. The use of  $^{40}\text{Ar}/^{39}\text{Ar}$  Ar data in evaluation of disturbed K-Ar systems, *U.S. Geol. Surv. Open-File Rept.*, **78-701**, 241–243.
- Lanphere, M.A., Champion, D.E., Christiansen, R.L., Izett, G.A. & Obradovich, J.D., 2002. Revised ages for tuffs of the Yellowstone Plateau volcanic field: assignment of the Huckleberry Ridge Tuff to a new geomagnetic polarity event, *Geol. Soc. Am. Bull.*, **114**, 559–568.
- Lipman, P.W., 1975. Evolution of Platoro Caldera Complex and related volcanic rocks, Southeastern San Juan Mountains, Colorado, *Geological Survey Professional Paper 852*, 128 pp.
- McFadden, P.L. & McElhinny, M.W., 1988. The combined analysis of remagnetization circles and direct observations in paleomagnetism, *Earth planet. Sci. Lett.*, **87**, 161–172.
- Mochizuki, N., Tsunakawa, H., Oishi, Y., Wakai, S., Wakabayashi, K. & Yamamoto, Y., 2004. Palaeointensity study of the Oshima 1986 lava in Japan: implications for the reliability of the Thellier and LTD-DHT Shaw methods, *Phys. Earth planet. Inter.*, **146**, 395–416.
- Mochizuki, N., Tsunakawa, H., Shibuya, H., Cassidy, J. & Smith, I.E.M., 2006. Palaeointensities of the Auckland geomagnetic excursions by the LTD-DHT Shaw method, *Phys. Earth planet. Inter.*, **154**, 168–179.
- McDougall, I., Brown, F.H., Cerling, T.E. & Hillhouse, J.W., 1992. A reappraisal of the geomagnetic polarity time scale to 4 Ma using data from the Turkana Basin, east Africa, *Geophys. Res. Lett.*, **19**, 2349–2352.
- Oda, H., 2005. Recurrent geomagnetic excursions: a review for the Brunhes normal polarity chron, *J. Geogra.*, **114**, 174–193 (Japanese with English abstract).
- Oishi, Y., Tsunakawa, H., Mochizuki, N., Yamamoto, Y., Wakabayashi, K. & Shibuya, H., 2005. Validity of the LTD-DHT Shaw and Thellier palaeointensity methods: a case study of the Kilauea 1970 lava, *Phys. Earth planet. Inter.*, **149**, 243–257.
- Ozima, M., Ozima, M. & Akimoto, S., 1964. Low temperature characteristics of remanent magnetization of magnetite—Self-reversal and recovery phenomena of remanent magnetization—, *J. Geomag. Geoelectr.*, **16**, 165–177.
- Renne, P., Walter, R., Verosub, K., Sweitzer, M. & Aronson, J., 1993. New data from Harder (Ethiopia) support orbitally tuned time scale to 3.3 Ma, *Geophys. Res. Lett.*, **20**, 1067–1070.
- Renne, P.R., WoldeGabriel, G., Hart, W.K., Heiken, G. & White, T.D., 1999. Chronostratigraphy of the Miocene-Pliocene Sagantole Formation, Middle Awash Valley, Afar rift, Ethiopia, *Geol. Soc. Am. Bull.*, **111**, 869–885.
- Roberts, A.P., Pike, C.R. & Verosub, K.L., 2000. First-order reversal curve diagrams: a new tool for characterizing the magnetic properties of natural samples, *J. geophys. Res.*, **105**, 28 461–28 475.
- Roger, S. et al., 2000.  $^{40}\text{Ar}/^{39}\text{Ar}$  dating of a tephra layer in the Pliocene Seneze maar lacustrine sequence (French Massif Central): constraint on the age of Reunion-Matuyama transition and implications for paleoenvironmental archives, *Earth planet. Sci. Lett.*, **183**, 431–440.
- Rolph, T.C. & Shaw, J., 1985. A new method of paleofield magnitude correction for thermally altered samples and its application to Lower Carboniferous lavas, *Geophys. J. R. astr. Soc.*, **80**, 773–781.
- Roperch, P. & Duncan, R.A., 1990. Records of geomagnetic reversals from volcanic islands of French Polynesia I. Paleomagnetic study of a polarity transition in a lava sequence from the island of Huahine, *J. geophys. Res.*, **95**, 2713–2726.
- Shackleton, N.J., Berger, A. & Peltier, W.R., 1990. An alternative astronomical calibration of the lower Pleistocene time scale based on ODP site 677, *Trans. R. Soc. Edinburgh Earth Sci.*, **81**, 251–261.
- Singer, B.S. & Brown, L.L., 2002. The Santa Rosa Event:  $^{40}\text{Ar}/^{39}\text{Ar}$  and paleomagnetic results from the Valles rhyolite near Jaramillo Creek, Jemez Mountains, New Mexico, *Earth planet. Sci. Lett.*, **197**, 51–64.
- Singer, B.S., Hoffman, K.A., Chauvin, A., Coe, R.S. & Pringle, M.S., 1999. Dating transitionally magnetized lavas of the late Matuyama Chron: toward a new  $^{40}\text{Ar}/^{39}\text{Ar}$  timescale of reversals and events, *J. geophys. Res.*, **104**, 679–693.
- Singer, B.S., Hoffman, K.A., Coe, R.S., Brown, L.L., Jicha, B.R., Pringle, M.S. & Chauvin, A., 2005. Structural and temporal requirements for geomagnetic field reversal deduced from lava flows, *Nature*, **434**, 633–636.
- Steiger, R.H. & Jäger, E., 1977. Subcommission on geochronology: convention on the use of decay constants in geo- and cosmochronology, *Earth planet. Sci. Lett.*, **36**, 359–362.
- Steven, T.A., Mehnert, H.H. & Obradovich, J.D., 1967. Age of Volcanic activity in the San Juan Mountains, Colorado, *U.S.G.S. Prof. Paper*, **575-D**, D47–D55.
- Tanaka, H., Turner, G.M., Houghton, B.F., Tachibana, T., Kono, M. & McWilliams, M.O., 1996. Palaeomagnetism and chronology of the central Taupo Volcanic Zone, New Zealand, *Geophys. J. Int.*, **124**, 919–934.
- Tauxe, L., 2006. Long-term trends in paleointensity: the contribution of DSDP/ODP submarine basaltic glass collections, *Phys. Earth planet. Inter.*, **156**, 223–241.
- Tsunakawa, H., Shimura, K. & Yamamoto, Y., 1997. Application of double heating technique of the Shaw method to the Brunhes epoch volcanic rocks (abstract), in *Proc. 8th Scientific Assembly IAGA, 1997 Abstract book*, pp. 85, Uppsala.
- Turrin, B.D., Donnelly-Nolan, J.M. & Cater Hearn, B., Jr, 1994.  $^{40}\text{Ar}/^{39}\text{Ar}$  Ar ages from the rhyolite of Alder Creek, California: age of the Cobb Mountain Normal-Polarity Subchron revisited, *Geology*, **22**, 251–254.
- Uchiyumi, S. & Shibata, K., 1980. Errors in K-Ar age determinations, *Bull. Geol. Surv. Japan*, **31**, 267–273 (in Japanese with English abstract).
- Udagawa, S., Kitagawa, H., Gudmundsson, A., Hiroi, O., Koyaguchi, T., Tanaka, H., Kristjansson, L. & Kono, M., 1999. Age and magnetism of lavas in Jokuldalur area, Eastern Iceland: gilsá event revisited, *Phys. Earth planet. Inter.*, **115**, 147–171.
- Uto, K., Ishizuka, O., Matsumoto, A., Kamioka, H. & Togashi, S., 1997. Laser-heating  $^{40}\text{Ar}/^{39}\text{Ar}$  dating system of the Geological Survey of Japan: system outlines and preliminary results, *Bull. Geol. Survey Japan*, **48**, 23–46.
- Valet, J.P., Meynadier, L. & Guyodo, Y., 2005. Geomagnetic dipole strength and reversal rate over the past two million years, *Nature*, **435**, 802–805.
- Verosub, K.L. & Banerjee, S.K., 1977. Geomagnetic excursions and their paleomagnetic record, *Rev. Geophys. Space Phys.*, **15**, 145–155.
- White, W.M. & Duncan, R.A., 1996. Geochemistry and Geochronology of the Society Islands: new evidence for deep mantle recycling, in *Earth Processes: Reading the Isotopic Code*, *Geophys. Monogr. Ser.*, Vol. 95, pp. 183–206, eds Basu, A. & Hart, S., AGU, Washington, DC.
- Whitney, J.A. & Stormer, J.C., 1985. Mineralogy, petrology, and magmatic conditions from the Fish Canyon Tuff, Central San Juan Volcanic Field, Colorado, *J. Petrol.*, **26**, 726–762.
- Yamamoto, Y. & Tsunakawa, H., 2005. Geomagnetic field intensity during the last 5 Myr: LTD-DHT Shaw palaeointensities from volcanic rocks of the Society Islands, French Polynesia, *Geophys. J. Int.*, **162**, 79–114.
- Yamamoto, Y. et al., 2002. Geomagnetic paleosecular variation for the past 5 Ma in the Society Islands, French Polynesia, *Earth Planets Space*, **54**, 797–802.
- Yamamoto, Y., Tsunakawa, H. & Shibuya, H., 2003. Palaeointensity study of the Hawaiian 1960 lava: implications for possible causes of erroneously high intensities, *Geophys. J. Int.*, **153**, 263–276.
- Yamazaki, T. & Oda, H., 2005. A geomagnetic paleointensity stack between 0.8 and 3.0 Ma from equatorial Pacific sediment cores, *Geochem. Geophys. Geosyst.*, **6**, Q11H20, doi:10.1029/2005GC001001.
- York, D., 1969. Least-squares fitting of a straight line with correlated errors, *Earth planet. Sci. Lett.*, **5**, 320–324.

**Table A1.** Appendix A: Results of isotopic analysis for  $^{40}\text{Ar}/^{39}\text{Ar}$  dating.

Laser output	$^{40}\text{Ar}/^{39}\text{Ar}$	$^{37}\text{Ar}/^{39}\text{Ar}$	$^{36}\text{Ar}/^{39}\text{Ar}$ ( $\times 10^{-3}$ )	Ca/K	$^{40}\text{Ar}^*$ (per cent)	$^{39}\text{Ar}_K$ fraction (per cent)	$^{40}\text{Ar}^*/^{39}\text{Ar}_K$	Age( $\pm 1\sigma$ ) (Ma)
RT05								
U05106 JMTR0401-1								
$J = 0.003177$								
0.52W	4.905 $\pm$ 0.105	1.915 $\pm$ 0.2319	0.8378 $\pm$ 0.0362	3.26	99.3	1.7	4.879 $\pm$ 0.109	27.75 $\pm$ 0.62
0.76W	1.494 $\pm$ 0.030	0.7780 $\pm$ 0.0891	3.483 $\pm$ 0.062	1.32	36.9	5.1	0.5518 $\pm$ 0.0274	3.16 $\pm$ 0.16
1.00W	1.169 $\pm$ 0.020	0.6805 $\pm$ 0.0668	2.506 $\pm$ 0.043	1.16	43.2	7.1	0.5051 $\pm$ 0.0196	2.89 $\pm$ 0.11
1.20W	0.9691 $\pm$ 0.0167	0.5199 $\pm$ 0.0731	1.808 $\pm$ 0.052	0.884	50.9	5.7	0.4932 $\pm$ 0.0210	2.82 $\pm$ 0.12
1.40W	1.473 $\pm$ 0.020	0.7858 $\pm$ 0.0794	3.488 $\pm$ 0.046	1.34	36.0	6.7	0.5307 $\pm$ 0.0199	3.04 $\pm$ 0.11
1.61W	1.129 $\pm$ 0.019	0.7170 $\pm$ 0.0740	2.370 $\pm$ 0.068	1.22	45.1	6.1	0.5094 $\pm$ 0.0252	2.92 $\pm$ 0.14
1.79W	1.254 $\pm$ 0.007	0.4363 $\pm$ 0.0639	2.772 $\pm$ 0.028	0.742	38.6	6.8	0.4841 $\pm$ 0.0118	2.77 $\pm$ 0.07
1.99W	0.8933 $\pm$ 0.0107	0.3601 $\pm$ 0.0942	1.514 $\pm$ 0.034	0.612	54.4	6.8	0.4862 $\pm$ 0.0166	2.78 $\pm$ 0.10
2.23W	0.9238 $\pm$ 0.0108	0.5180 $\pm$ 0.0482	1.633 $\pm$ 0.029	0.881	54.0	8.5	0.4994 $\pm$ 0.0128	2.86 $\pm$ 0.07
2.51W	0.7137 $\pm$ 0.0096	0.4591 $\pm$ 0.0642	0.9697 $\pm$ 0.0235	0.781	67.0	7.9	0.4786 $\pm$ 0.0127	2.74 $\pm$ 0.07
2.88W	0.7049 $\pm$ 0.0093	0.5475 $\pm$ 0.0260	0.9466 $\pm$ 0.0125	0.931	69.0	17.0	0.4866 $\pm$ 0.0089	2.79 $\pm$ 0.05
3.30W	0.5532 $\pm$ 0.0066	0.5416 $\pm$ 0.0288	0.4725 $\pm$ 0.0080	0.921	85.7	20.6	0.4742 $\pm$ 0.0072	2.72 $\pm$ 0.04
RT10								
U05107 JMTR0401-1								
$J = 0.003073$								
0.52W	1.375 $\pm$ 0.019	2.414 $\pm$ 0.428	3.382 $\pm$ 0.152	4.11	46.9	1.4	0.6465 $\pm$ 0.0669	3.58 $\pm$ 0.37
0.77W	0.6999 $\pm$ 0.0116	1.032 $\pm$ 0.098	0.9799 $\pm$ 0.0377	1.76	75.1	4.3	0.5260 $\pm$ 0.0185	2.91 $\pm$ 0.10
1.00W	0.6089 $\pm$ 0.0127	0.9491 $\pm$ 0.0714	0.6307 $\pm$ 0.0336	1.61	86.8	5.3	0.5289 $\pm$ 0.0173	2.93 $\pm$ 0.10
1.24W	0.6317 $\pm$ 0.0050	0.8729 $\pm$ 0.0871	0.7460 $\pm$ 0.0226	1.49	80.5	6.7	0.5092 $\pm$ 0.0126	2.82 $\pm$ 0.07
1.48W	0.5873 $\pm$ 0.0058	0.8726 $\pm$ 0.0885	0.6148 $\pm$ 0.0312	1.48	85.7	6.4	0.5034 $\pm$ 0.0145	2.79 $\pm$ 0.08
1.74W	0.5683 $\pm$ 0.0070	0.8893 $\pm$ 0.0664	0.5467 $\pm$ 0.0227	1.51	89.1	7.6	0.5064 $\pm$ 0.0119	2.81 $\pm$ 0.07
1.99W	0.5471 $\pm$ 0.0058	1.175 $\pm$ 0.095	0.5417 $\pm$ 0.0223	2.00	94.7	6.8	0.5188 $\pm$ 0.0137	2.87 $\pm$ 0.08
2.20W	0.5512 $\pm$ 0.0072	1.040 $\pm$ 0.066	0.5816 $\pm$ 0.0156	1.77	89.9	8.5	0.4960 $\pm$ 0.0110	2.75 $\pm$ 0.06
2.35W	0.5513 $\pm$ 0.0075	1.099 $\pm$ 0.103	0.6296 $\pm$ 0.0270	1.87	88.5	5.3	0.4885 $\pm$ 0.0156	2.71 $\pm$ 0.09
2.58W	0.5569 $\pm$ 0.0082	1.291 $\pm$ 0.100	0.7023 $\pm$ 0.0329	2.20	88.6	5.6	0.4942 $\pm$ 0.0166	2.74 $\pm$ 0.09
2.90W	0.5264 $\pm$ 0.0026	0.8954 $\pm$ 0.0348	0.5022 $\pm$ 0.0078	1.52	90.8	16.9	0.4783 $\pm$ 0.0052	2.65 $\pm$ 0.03
3.12W	0.5227 $\pm$ 0.0053	1.155 $\pm$ 0.061	0.6114 $\pm$ 0.0185	1.97	90.1	13.3	0.4715 $\pm$ 0.0101	2.61 $\pm$ 0.06
3.34W	0.5443 $\pm$ 0.0015	1.674 $\pm$ 0.166	0.8993 $\pm$ 0.0488	2.85	85.5	4.6	0.4661 $\pm$ 0.0236	2.58 $\pm$ 0.13
3.74W	0.5802 $\pm$ 0.0067	2.608 $\pm$ 0.093	1.310 $\pm$ 0.026	4.44	83.5	7.2	0.4853 $\pm$ 0.0141	2.69 $\pm$ 0.08
TA04								
U05101 JMTR0401-1								
$J = 0.003098$								
0.50W	1.440 $\pm$ 0.024	6.540 $\pm$ 1.306	4.689 $\pm$ 0.393	11.2	54.5	0.9	0.7892 $\pm$ 0.1882	4.41 $\pm$ 1.05
0.69W	0.8542 $\pm$ 0.0133	1.603 $\pm$ 0.444	1.460 $\pm$ 0.123	2.73	70.5	2.4	0.6028 $\pm$ 0.0625	3.37 $\pm$ 0.35
0.90W	0.7365 $\pm$ 0.0157	1.382 $\pm$ 0.223	0.9919 $\pm$ 0.0457	2.35	81.2	4.1	0.5984 $\pm$ 0.0315	3.34 $\pm$ 0.18
1.06W	0.7252 $\pm$ 0.0122	1.235 $\pm$ 0.220	0.9602 $\pm$ 0.0669	2.10	79.9	4.0	0.5800 $\pm$ 0.0333	3.24 $\pm$ 0.19
1.19W	0.7342 $\pm$ 0.0124	1.274 $\pm$ 0.179	0.9989 $\pm$ 0.0864	2.17	79.2	3.5	0.5820 $\pm$ 0.0343	3.25 $\pm$ 0.19
1.30W	0.7264 $\pm$ 0.0133	1.463 $\pm$ 0.134	0.9808 $\pm$ 0.0676	2.49	82.6	4.3	0.6007 $\pm$ 0.0276	3.35 $\pm$ 0.15
1.40W	0.7236 $\pm$ 0.0122	1.219 $\pm$ 0.179	0.9268 $\pm$ 0.0648	2.07	81.0	3.6	0.5864 $\pm$ 0.0298	3.27 $\pm$ 0.17
1.52W	0.7142 $\pm$ 0.0109	1.266 $\pm$ 0.150	0.8339 $\pm$ 0.0409	2.15	85.3	5.3	0.6098 $\pm$ 0.0229	3.41 $\pm$ 0.13
1.63W	0.7150 $\pm$ 0.0118	1.535 $\pm$ 0.147	0.9895 $\pm$ 0.0701	2.61	83.1	5.1	0.5949 $\pm$ 0.0284	3.32 $\pm$ 0.16
1.76W	0.6924 $\pm$ 0.0136	1.350 $\pm$ 0.089	0.8596 $\pm$ 0.0507	2.30	85.1	4.7	0.5898 $\pm$ 0.0218	3.29 $\pm$ 0.12
1.90W	0.6835 $\pm$ 0.0091	1.105 $\pm$ 0.191	0.7902 $\pm$ 0.0513	1.88	83.9	5.4	0.5740 $\pm$ 0.0274	3.21 $\pm$ 0.15
2.07W	0.7023 $\pm$ 0.0117	1.451 $\pm$ 0.292	0.8585 $\pm$ 0.0721	2.47	87.0	5.0	0.6115 $\pm$ 0.0404	3.41 $\pm$ 0.23
2.24W	0.7457 $\pm$ 0.0097	1.358 $\pm$ 0.173	1.102 $\pm$ 0.065	2.31	76.7	5.3	0.5725 $\pm$ 0.0284	3.20 $\pm$ 0.16
2.42W	0.6800 $\pm$ 0.0116	1.396 $\pm$ 0.159	0.8286 $\pm$ 0.0693	2.38	86.9	5.8	0.5917 $\pm$ 0.0290	3.30 $\pm$ 0.16
2.60W	0.6569 $\pm$ 0.0110	1.080 $\pm$ 0.199	0.7683 $\pm$ 0.0481	1.84	83.8	5.0	0.5510 $\pm$ 0.0282	3.08 $\pm$ 0.16
2.82W	0.6428 $\pm$ 0.0090	1.123 $\pm$ 0.062	0.6852 $\pm$ 0.0319	1.91	88.0	10.7	0.5663 $\pm$ 0.0144	3.16 $\pm$ 0.08
3.02W	0.6479 $\pm$ 0.0094	1.322 $\pm$ 0.062	0.8545 $\pm$ 0.0275	2.25	83.8	13.8	0.5437 $\pm$ 0.0135	3.04 $\pm$ 0.08
3.26W	0.6732 $\pm$ 0.0098	1.815 $\pm$ 0.119	1.125 $\pm$ 0.032	3.09	80.8	11.1	0.5445 $\pm$ 0.0183	3.04 $\pm$ 0.10

**Table A1.** (Continued.)

Laser output	<sup>40</sup> Ar/ <sup>39</sup> Ar	<sup>37</sup> Ar/ <sup>39</sup> Ar	<sup>36</sup> Ar/ <sup>39</sup> Ar (× 10 <sup>-3</sup> )	Ca/K	<sup>40</sup> Ar* (per cent)	<sup>39</sup> Ar <sub>K</sub> fraction (per cent)	<sup>40</sup> Ar* / <sup>39</sup> Ar <sub>K</sub>	Age(±1σ) (Ma)
TA05								
U05104 JMTR0401-1								
<i>J</i> = 0.002991								
0.49W	1.731 ± 0.036	2.529 ± 0.325	3.913 ± 0.109	4.31	49.5	1.0	0.8585 ± 0.0545	4.63 ± 0.29
0.70W	0.9892 ± 0.0259	0.7304 ± 0.1110	1.398 ± 0.054	1.24	66.5	3.6	0.6582 ± 0.0291	3.55 ± 0.16
0.84W	0.8657 ± 0.0230	0.5485 ± 0.2198	1.073 ± 0.027	0.933	70.5	3.2	0.6103 ± 0.0322	3.29 ± 0.17
0.97W	0.9003 ± 0.0226	0.5490 ± 0.1744	1.129 ± 0.057	0.934	69.8	2.6	0.6283 ± 0.0320	3.39 ± 0.17
1.09W	0.8986 ± 0.0112	0.2492 ± 0.1215	1.148 ± 0.049	0.424	65.4	3.5	0.5873 ± 0.0219	3.17 ± 0.12
1.23W	0.8928 ± 0.0116	0.3521 ± 0.0986	1.009 ± 0.039	0.599	71.0	3.3	0.6341 ± 0.0187	3.42 ± 0.10
1.35W	0.8478 ± 0.0138	0.4776 ± 0.1143	0.9647 ± 0.0318	0.812	72.7	2.8	0.6163 ± 0.0198	3.32 ± 0.11
1.50W	0.8094 ± 0.0106	0.3941 ± 0.1266	0.8748 ± 0.0401	0.670	73.5	3.3	0.5951 ± 0.0206	3.21 ± 0.11
1.67W	0.8067 ± 0.0130	0.4244 ± 0.0859	0.8169 ± 0.0259	0.722	76.0	4.8	0.6130 ± 0.0167	3.30 ± 0.09
1.81W	0.7741 ± 0.0135	0.3836 ± 0.0992	0.7548 ± 0.0186	0.652	76.7	4.4	0.5941 ± 0.0171	3.20 ± 0.09
1.96W	0.7849 ± 0.0160	0.5398 ± 0.1008	0.8088 ± 0.0241	0.918	77.2	4.8	0.6065 ± 0.0193	3.27 ± 0.10
2.12W	0.7634 ± 0.0156	0.4956 ± 0.1308	0.7776 ± 0.0315	0.843	77.2	4.2	0.5892 ± 0.0221	3.18 ± 0.12
2.31W	0.7715 ± 0.0134	0.5714 ± 0.1159	0.7682 ± 0.0235	0.972	78.8	5.9	0.6086 ± 0.0189	3.28 ± 0.10
2.51W	0.8038 ± 0.0163	0.6426 ± 0.1028	0.9349 ± 0.0259	1.09	74.6	5.7	0.5996 ± 0.0196	3.23 ± 0.11
2.72W	0.7234 ± 0.0051	0.6583 ± 0.0299	0.6811 ± 0.0235	1.12	82.3	8.1	0.5960 ± 0.0090	3.21 ± 0.05
2.93W	0.7365 ± 0.0085	0.4803 ± 0.0318	0.6777 ± 0.0148	0.817	80.1	11.3	0.5901 ± 0.0094	3.18 ± 0.05
3.18W	0.7103 ± 0.0087	0.5286 ± 0.0332	0.6259 ± 0.0126	0.899	82.3	11.6	0.5847 ± 0.0094	3.15 ± 0.05
3.49W	0.7181 ± 0.0083	0.7522 ± 0.0295	0.7172 ± 0.0175	1.28	82.2	15.8	0.5906 ± 0.0096	3.18 ± 0.05
MP01								
U05105 JMTR0401-1								
<i>J</i> = 0.003025								
0.51W	1.132 ± 0.018	0.1660 ± 0.1932	0.9462 ± 0.0660	3.54	76.9	0.8	0.8706 ± 0.0333	4.74 ± 0.18
0.76W	0.8928 ± 0.0076	0.0813 ± 0.0345	0.2799 ± 0.0148	7.23	91.8	3.0	0.8192 ± 0.0093	4.47 ± 0.05
0.91W	0.8504 ± 0.0061	0.0771 ± 0.0232	0.1803 ± 0.0140	7.63	94.7	3.4	0.8059 ± 0.0077	4.39 ± 0.04
1.05W	0.8368 ± 0.0061	0.0809 ± 0.0459	0.1558 ± 0.0137	7.27	95.6	3.4	0.7999 ± 0.0089	4.36 ± 0.05
1.20W	0.8393 ± 0.0069	0.1074 ± 0.0350	0.1316 ± 0.0092	5.47	96.8	3.8	0.8125 ± 0.0083	4.43 ± 0.05
1.35W	0.8397 ± 0.0061	0.1384 ± 0.0448	0.1380 ± 0.0184	4.25	97.0	3.5	0.8145 ± 0.0095	4.44 ± 0.05
1.51W	0.8372 ± 0.0064	0.0930 ± 0.0315	0.1422 ± 0.0117	6.32	96.2	4.4	0.8056 ± 0.0080	4.39 ± 0.05
1.70W	0.8358 ± 0.0100	0.1244 ± 0.0228	0.1316 ± 0.0075	4.73	97.0	4.8	0.8109 ± 0.0104	4.42 ± 0.06
1.88W	0.8324 ± 0.0108	0.0969 ± 0.0255	0.1090 ± 0.0082	6.07	97.4	4.7	0.8111 ± 0.0113	4.42 ± 0.06
2.11W	0.8300 ± 0.0101	0.0858 ± 0.0328	0.1085 ± 0.0107	6.85	97.3	6.2	0.8076 ± 0.0110	4.40 ± 0.06
2.31W	0.8261 ± 0.0051	0.0821 ± 0.0369	0.0864 ± 0.0071	7.17	98.0	5.1	0.8098 ± 0.0068	4.41 ± 0.04
2.60W	0.8223 ± 0.0117	0.1087 ± 0.0198	0.0927 ± 0.0065	5.41	98.1	7.0	0.8072 ± 0.0120	4.40 ± 0.07
2.91W	0.8185 ± 0.0052	0.1100 ± 0.0203	0.0875 ± 0.0050	5.35	98.3	7.1	0.8050 ± 0.0058	4.39 ± 0.03
3.21W	0.8220 ± 0.0039	0.1118 ± 0.0269	0.0946 ± 0.0052	5.26	98.1	7.8	0.8066 ± 0.0051	4.40 ± 0.03
3.51W	0.8170 ± 0.0014	0.1599 ± 0.0062	0.0914 ± 0.0023	3.68	98.9	20.9	0.8080 ± 0.0017	4.40 ± 0.02
3.83W	0.8115 ± 0.0014	0.1895 ± 0.0070	0.0888 ± 0.0020	3.10	99.4	14.0	0.8065 ± 0.0017	4.40 ± 0.02

\* U05101-U05107: Measurement IDs in the laboratory.

\* JMTR0401-1: Irradiation numbers in the laboratory.